RESEARCH ARTICLE | JULY 12 2021

Free-surface effects induced by internal solitons forced by shearing currents

Giovanni la Forgia ; Giampiero Sciortino

Physics of Fluids 33, 072102 (2021)
https://doi.org/10.1063/5.0055466

Physics of Fluids ARTICLE scitation.org/journal/phf

Free-surface effects induced by internal solitons forced by shearing currents

Cite as: Phys. Fluids **33**, 072102 (2021); doi: 10.1063/5.0055466
Submitted: 29 April 2021 · Accepted: 18 June 2021 ·
Published Online: 12 July 2021

Giovanni la Forgia[1,2,a] and Giampiero Sciortino[3]

AFFILIATIONS

[1]Institute of Marine Sciences, National Research Council, 00133 Rome, Italy
[2]Department of Civil and Mechanical Engineering, University of Cassino and Southern Lazio, Cassino 03043, Italy
[3]Department of Engineering, Roma Tre University, 00146 Rome, Italy

[a]Author to whom correspondence should be addressed: giovanni.laforgia@uniroma3.it

ABSTRACT

Free-surface effects induced by internal solitary waves (ISWs) propagating through a background shear current are theoretically investigated in a shallow water framework. Following the Hamiltonian approach, we implement a mathematical formulation valid for a free surface, two-layer stratified system in the presence of mobile layers. Associated to the undisturbed condition characterized by the background fluid at rest, solitons with both positive and negative polarities are considered. To reproduce the typical oceanic conditions, we focus on theoretical predictions for a density ratio set to 0.99. Although under Boussinesq conditions a rigid-lid at the top of the theoretical domain is considered a good approximation, our analysis shows that main ISWs features may change when the fluid system, forced by shear currents, is modeled with a free surface. Signs assumed by three dimensionless quantities, i.e., the deformation parameter, the background velocity, and the undisturbed amplitude, allowed us to uniquely predict how the undisturbed solitons modify their interfacial profiles and change their celerity, in response to the background forcing. Our results show that waves celerity predicted by the rigid-lid model can be lower than the one resulting from the Hamiltonian formulation, although this never occurs in the absence of mobile layers. Theoretical predictions reveal that shearing current can induce deviations from the standard ISWs free-surface profile. We discuss the role of nonhydrostatic pressures in inducing free-surface short disturbances, in the form of undulated or multihumped profiles. The typical phase-opposition between interfacial and surface displacements can be lost as the free-surface displacements assume multihumped configurations.

I. INTRODUCTION

Internal solitary waves (ISWs) represent widespread phenomena in density-stratified fluid environments, particularly in the coastal ocean. They propagate along the pycnocline, a relatively thin layer characterized by strong, vertical density gradient due to abrupt changes in water temperature or salinity between the surrounding water layers.[1,2] Although ISWs can be induced by lee waves, resonance, and river outflows,[3–10] they are mainly generated by the interaction between tidal currents and rough features of the seabed topography, such as continental slopes, ridges, sea mounts, and canyons.[11,12] Nowadays, ISWs represent one of the most investigated phenomena within the continental shelf/slope for their crucial role in sediment resuspension/redistribution, turbulence and mixing induced by their breaking.[13–19]

Real field observations showed that these waves can travel for long distances preserving their shape and celerity, due to a balance between dispersive spreading and nonlinear steepening.[20,21] At the free surface (FS), convergent and divergent zones are observed to move in phase with ISWs troughs, inducing a superficial roughness that appears as distinctive features in synthetic aperture radar (SAR) imagery.[20,22]

The simplest theoretical models able to describe the propagation of ISWs refer to the weakly nonlinear theories, such as the Korteweg–de Vries (KdV) model.[23] Numerical integration of the KdV equation proved that a large–amplitude initial sine wave dissolved into a sequence of solitary waves. Since these waves collided elastically rematerializing their precollision amplitudes and widths they were called *solitons*.[24] Strictly speaking, the term *soliton* is reserved for ISWs in integrable systems, but we will nevertheless follow the widely used custom and call these waves *internal solitons*.[25]

To accurately describe properties of oceanic observations of relatively large-amplitude ISWs, higher-order nonlinear models were developed, such as the strongly nonlinear, weakly dispersive Miyata–Choi–Camassa model (*MCC*).[26,27] Theoretical, numerical and laboratory studies performed in the past assumed the rigid-lid (RL) approximation or adopted a density difference too low to induce

surface manifestations.[28–31] For the first time, Kodaira *et al.*[32] investigated large-amplitude internal solitary waves propagating under the top free surface in a two-layer stratified system with uniform densities. By using two immiscible fluids with a non-negligible density jump at the interface, they compared experimental results with those obtained by the *MCC* model, under both the free-surface (*FS*) and rigid-lid (*RL*) approximations. They found that the strongly nonlinear *MCC-FS* model agrees better with the measurements proving that the free-surface boundary condition at the top surface is crucial in describing the internal solitary waves in the experiment correctly. More recently, with a similar experimental setting and theoretical analysis la Forgia and Sciortino[33] highlighted that the existence of a free surface allows the ISWs to transfer part of their energy to the free surface, such that the wave celerity assumed lower values with respect to solitons speed resulting from the *MCC-RL* model. These studies showed that for constant background environments in terms of stratification and currents, the interfacial and the surface displacements of internal solitons of elevation and depression, always propagate in phase opposition; moreover, the surface manifestation associated with the internal wave is always composed of a single-hump shaped, solitary wave-like profile.

By using Hamilton's principle, Barros and Gavrilyuk[34] derived stationary solutions for the approximate model developed by Barros, Gavrilyuk, and Teshukov,[35] describing large-amplitude long waves in two-layer flows with a free surface. Far from the Boussinesq conditions (i.e., for an unrealistic density ratio $\rho = 0.1$), their model predicted multihump shaped profiles for both the interface and the free surface. However, they showed that under oceanic conditions ($\rho = 0.99$), both the internal interface and the free surface always present a single-hump shaped profile. Of particular interest are model prediction of multihumped solitons, although observed only for unrealistic stratified configurations.

Tidal-generated ISWs are often observed to propagate in stratified ambients in the presence of a not uniform distribution of the background velocities, and recent studies focused on solitons features as they propagate through shear currents.[36–38] Theoretical investigations performed by Choi[39] first analyzed the steady solution of the ISWs in linear shear flow, showing that for negative ambient vorticity, a solitary wave of depression, traveling in the positive x-direction, is wider and slower with respect to the case of an irrotational environment. Moreover, ISWs of depression are observed to be narrower and faster when traveling in the negative x-direction. Through a variational algorithm, Stastna and Lamb[38] investigated the effects of a nonuniform background shear current on properties of large-amplitude ISWs in a shallow, stratified ambient. They found that amplitudes of soliton of elevation increase with the background vorticity, implying that, for background currents with negative vorticity, rightward-propagating waves are much wider than the case with the fluid ambient at-rest. By high-resolution direct numerical simulations, Xu and Stastna[40] studied ISWs of depression propagating in a quasi-two-layer stratification with a shear background current. They showed that solitons assume a smaller amplitude and a larger half-width if the background vorticity has the same sign as the ISW-induced vorticity. More recently, la Forgia and Sciortino[41] analyzed soliton solution derived by a new version of the *MCC-RL* model with mobile layers, i.e., the *MCC-ML* model. Under Boussinesq conditions they showed that ISWs interacting with a shearing current may reach critical stages that lead these waves to convert their polarity, to invert the original direction of propagation or to travel with amplitude equal to zero.

Although the rigid-lid condition is commonly considered a good approximation for simulating real field conditions, at the best of our knowledge, no studies focused on the effective role played by the free surface in modifying the soliton features in the presence of a background shear, under oceanic conditions. By following the Hamiltonian approach proposed by Barros, Gavrilyuk, and Teshukov,[35] in the present paper, we develop a theoretical formulation based on the Hamiltonian approach (*H*), for a fluid system with a Free Surface (*FS*) and two Mobile Layers (*ML*) composing the background. For the sake of brevity, we define this formulation as *HFS-ML* model. It allowed us to find soliton solutions in the presence of a shear background current in a two-layer stratified ambient with a free surface. We used Wolfram MATHEMATICA both to compute the solutions by means of the built-in function NDSolve,[42] and to perform complex symbolic algebraic manipulations. Our main goal is to theoretically investigate the strain behavior of both the interfacial and surface displacement associated with ISWs forced by an even larger background shearing current. We analyzed theoretical prediction provided by the *HFS-ML* model in order to study how soliton features may be affected by the presence of the free surface for increasing shear currents acting at the background. In particular, we consider a real field density configuration, by setting the density ratio between the two layers equal to 0.99; then we vary the ratio of the undisturbed layer thickness from 0.1 to 10, in order to compare our results with those obtained under the rigid-lid assumption by la Forgia and Sciortino.[41] We develop the *HFS-ML* model and we analyzed the associated theoretical predictions for real field conditions in order to provide answers to the following scientific questions:

- compared to the rigid-lid approximation, how the presence of the free surface modifies soliton main features?
- how the free-surface displacement evolves for increasing shear currents?
- does the surface displacement preserve the standard single-hump shaped profile, i.e., the one typically observed in the real field when the background fluid is at-rest?

Our investigation and related results are valid only for real field conditions that can be effectively schematized by a two-layer stratified system. For more realistic density distributions, more complex theoretical approaches should be considered (e.g., multilayer configurations[43,44]). The resulting ISWs, indeed, could be significantly different and higher mode internal waves are expected to develop. We remark that stability of soliton solutions provided by the *HFS-ML* model is not discussed in the present work. Among the complex approaches that could be adopted, we just mention the Melnikov method, which allows to identify the existence of chaotic orbits in a class of dynamical systems under periodic perturbation.[45–47]

The remainder of the paper is organized as follows. In Sec. II, we describe the model equations for ISWs propagating in a stratified two-layer fluid system with a free surface; Sec. III presents the main findings in terms of evolution of ISWs profiles for both increasing background shear and ambient stratifications. We show how the main ISWs features change with respect to predictions derived by the rigid-lid model. Furthermore, we provide a physical explanation for the observed nonstandard surface displacements, highlighting the stratification conditions that enhance their generation. Finally, a general discussion and concluding remarks are inferred in Sec. IV.

II. THEORETICAL MODEL

A. Free-surface model with Hamiltonian approach

We consider a stratified system composed of two uniform layers: a lower layer of thickness h_1 and density ρ_1, and a lighter layer of thickness h_2 with density $\rho_2 < \rho_1$ (Fig. 1). In the shallow-water framework, two different but equivalent approaches have been developed for modeling interfacial solitons with a free surface: the *MCC-FS* model[48] and the Barros formulation.[34,35] To account for the free surface, both methods remove the rigid-lid assumption, namely that the sum of the local thicknesses $\eta_1 + \eta_2$ has to be constant. With respect to the undisturbed, at-rest condition, the ISW-induced interfacial and surface displacements are ζ_1 and ζ_2, respectively (Fig. 1). The local thicknesses η_1, η_2 are then defined as

$$\begin{cases} \eta_1 = h_1 + \zeta_1, \\ \eta_2 = h_2 + \zeta_2 - \zeta_1. \end{cases} \tag{1}$$

In agreement with Kodaira *et al.*,[32] paying attention to the reverse layers name notation they adopted, the continuity and momentum equations for each layer ($i = 1, 2$) can be written as

$$\begin{cases} \dfrac{\partial \eta_i}{\partial t} + \dfrac{\partial (u_i \eta_i)}{\partial x} = 0, \\ D_i u_i + g \dfrac{\partial (\eta_1 + \rho_2 \eta_2 / \rho_i)}{\partial x} = disp_i, \end{cases} \tag{2}$$

where $u_i = u_i(x,t)$ are the depth-averaged horizontal velocity, g is the gravitational acceleration, while $D_i \equiv \partial/\partial t + u_i \partial/\partial x$ and $disp_i$ represent nonlinear dispersive terms (see the Appendix). For differential system (2), soliton solutions of the form $\eta_i = \eta_i(X), u_i = u_i(X), X \equiv (x - ct)$ ($i = 1, 2$) can be obtained by integrating the continuity equations for each layer and imposing as boundary conditions at infinity, ($\eta_i \to h_i, u_i \to u_{0i}$ for $X \to \pm\infty$). In agreement with la Forgia and Sciortino,[41] it is easy to verify that

$$u_i = c(1 - h_i/\eta_i) + u_{0i} h_i/\eta_i, \tag{3}$$

where $u_{si} = c(1 - h_i/\eta_i)$ and $u_{bi} = u_{0i} h_i/\eta_i$ represent the soliton-induced and the background ambient-induced layers velocities, respectively. Thus, a *nonlinear second order differential system* of equations in the unknowns $\eta_i(X)$ can be derived.[32,33]

Following the elegant *Hamiltonian* approach proposed by Barros, Gavrilyuk, and Teshukov,[35] we implement the free-surface model for interfacial solitons by considering the effect of mobile layers with asymptotic velocity u_{01}, u_{02}, herein defined as *HFS-ML* model. We thus introduce the *Lagrangian* density $\mathcal{L}$ of the two-layer fluid system for the soliton configuration,

$$\mathcal{L}(\mathbf{Q}, \mathbf{Q}') \equiv T(\mathbf{Q}, \mathbf{Q}') - V(\mathbf{Q}), \tag{4}$$

where $T(\mathbf{Q}, \mathbf{Q}') \equiv \frac{1}{2}(\mathbf{Q}' \mathcal{M}(\mathbf{Q})) \cdot \mathbf{Q}'$ is the kinetic energy density, $(\bigcirc)'$ denotes derivative with respect to X, and " $\cdot$ " is the usual dot product. The *Lagrangian* density has *physical dimensions* $[\mathcal{L}] = MT^{-2}$. The *state variables* of the fluid system are

$$\mathbf{Q}(X) \equiv (Q_1(X), Q_2((X)) \equiv (\rho_1 \eta_1(X), \rho_2 \eta_2(X))$$

while $\mathbf{Q}' \mathcal{M}(\mathbf{Q})$ is the matrix multiplication between the *row-vector* $\mathbf{Q}'$ and the 2×2 symmetric matrix M defined by

$$\mathcal{M}(\mathbf{Q}) \equiv \begin{pmatrix} \dfrac{m_1^2}{3\rho_1^2 Q_1} + \dfrac{m_2^2}{\rho_1^2 Q_2} & \dfrac{m_2^2}{2\rho_1 \rho_2 Q_2} \\ \dfrac{m_2^2}{2\rho_1 \rho_2 Q_2} & \dfrac{m_2^2}{3\rho_2^2 Q_2} \end{pmatrix}. \tag{5}$$

The potential energy density $V(\mathbf{Q})$ is defined as

$$V(\mathbf{Q}) \equiv \frac{g}{2}\left(\frac{Q_1^2}{\rho_1} + 2\frac{Q_1 Q_2}{\rho_1} + \frac{Q_2^2}{\rho_2}\right) - \left(\frac{m_1^2}{2Q_1} + \frac{m_2^2}{2Q_2} + c_1 Q_1 + c_2 Q_2\right), \tag{6}$$

where m_1, m_2, c_1, c_2 are suitable constants[34,35] defined by

$$\begin{cases} m_i \equiv (u_{0i} - c)\rho_i h_i, \\ c_i \equiv g\left(h_1 + \dfrac{\rho_2 h_2}{\rho_i}\right) + \dfrac{1}{2}\left(\dfrac{m_i}{\rho_i h_i}\right)^2. \end{cases}$$

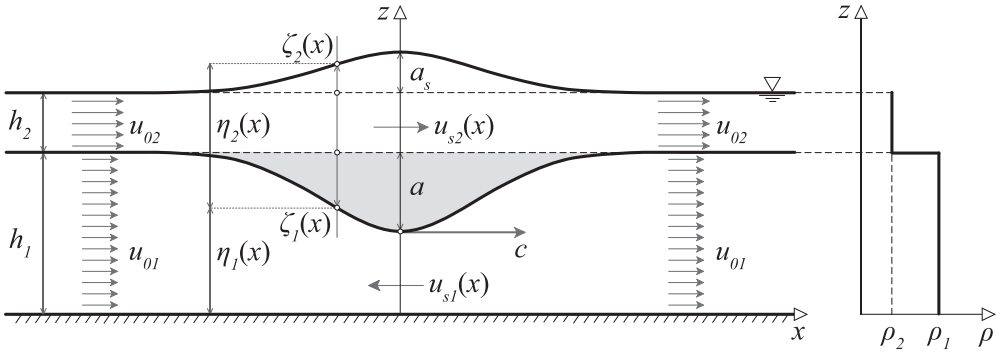

FIG. 1. Sketch of the ambient density and velocity distributions in the plane (x, z); the main geometric parameters defined to describe the interfacial and the surface displacements for the free-surface model with mobile layers are reported for the upper ($i = 2$) and lower ($i = 1$) layers: the asymptotic background velocities u_{0i}, the layers thickness h_i and uniform densities ρ_i, the local interfacial thickness η_i and the ISW-induced velocities $u_{si}(x)$. The dashed area indicates the internal soliton area S_s, ζ_i are the surface and interfacial displacements with respect to the undisturbed condition, while a and a_s are the interfacial and superficial amplitudes, respectively.

Let us to introduce the *conjugate momenta* $\mathbf{P} \equiv \partial\mathcal{L}/\partial\mathbf{Q}' = \mathbf{Q}'\mathcal{M}(\mathbf{Q})$ of the state variable $\mathbf{Q}$ in order to construct the Hamiltonian of the fluid system $\mathcal{H}$ defined by

$$\mathcal{H}(\mathbf{Q},\mathbf{P}) \equiv \mathbf{P}\cdot\mathbf{Q}' - \mathcal{L} = T + V = \frac{1}{2}\mathbf{P}\cdot(\mathbf{P}\mathcal{M}^{-1}) + V(\mathbf{Q}), \quad (7)$$

where the kinetic energy density $\frac{1}{2}(\mathbf{Q}'\mathcal{M})\cdot\mathbf{Q}'$ is written in terms of the conjugate momenta $\mathbf{P}$ as $\mathbf{Q}' = \mathbf{P}\mathcal{M}^{-1}$. Thus, the evolution-equations of the interfacial solitons are

$$\begin{cases} \mathbf{Q}' = \partial\mathcal{H}(\mathbf{Q},\mathbf{P})/\partial\mathbf{P}, \\ \mathbf{P}' = -\partial\mathcal{H}(\mathbf{Q},\mathbf{P})/\partial\mathbf{Q}, \end{cases} \quad (8)$$

which represent the well-known *first-order differential Hamilton's equations*, in the unknowns $(\mathbf{Q}(X),\mathbf{P}(X))$.

B. Dimensionless form of the mathematical model

Let us to introduce the following dimensionless physical quantities:

$$\begin{cases} \rho \equiv \rho_2/\rho_1, \quad H \equiv h_2/h_1, \quad Fr \equiv c/\sqrt{gh_1}, \quad \xi \equiv X/h_1, \\ q_i(\xi) \equiv \dfrac{Q_i(h_1\xi)}{\rho_i h_i} = \dfrac{\eta_i}{h_i}, \quad p_i(\xi) \equiv \dfrac{P_i(h_1\xi)}{gh_1h_i}, \quad Fr_{0i} \equiv u_{0i}/\sqrt{gh_1}, \end{cases} \quad (9)$$

where q_2, p_2 can be also written in terms of (ρ_1,h_1,g) and (ρ,H,Fr), respectively,

$$\begin{cases} q_2 \equiv \dfrac{Q_2}{\rho_2 h_2} = \dfrac{Q_2}{\rho_1 h_1 \frac{\rho_2}{\rho_1}\frac{h_2}{h_1}} = \dfrac{Q_2}{\rho_1 h_1 \rho H}, \\ p_2 \equiv \dfrac{P_2}{gh_1h_2} = \dfrac{P_2}{gh_1h_1\frac{h_2}{h_1}} = \dfrac{P_2}{Hgh_1^2}. \end{cases}$$

By substituting dimensionless quantities (9) in (7), after some heavy algebraic manipulation, it is possible to transform the Hamiltonian $\mathcal{H}$ into the new conserved quantity $\mathcal{H}_d(\mathbf{q},\mathbf{p},Fr)$, with $\mathbf{q} \equiv (q_1,q_2)$, $\mathbf{p} \equiv (p_1,p_2)$,

$$\begin{cases} \mathcal{H}_d(\mathbf{q},\mathbf{p},Fr) = \mathcal{T}_d(\mathbf{q},\mathbf{p},Fr) + \mathcal{V}_d(\mathbf{q},Fr), \\ \mathcal{T}_d(\mathbf{q},\mathbf{p},Fr) \equiv \dfrac{3(2p_1-3\rho Hp_2)^2}{4(Fr-Fr_{01})^2}q_1 + \rho H\dfrac{3p_2^2}{(Fr-Fr_{02})^2}q_2 - \dfrac{9(Fr-Fr_{02})^2\rho H(2p_1-3\rho Hp_2)^2q_1^2}{12(Fr-Fr_{01})^2(Fr-Fr_{02})^2\rho Hq_1+16(Fr-Fr_{01})^4q_2}, \\ \mathcal{V}_d(\mathbf{q},Fr) \equiv 1 + 2(Fr-Fr_{01})^2 + \rho H\big[2+2(Fr-Fr_{02})^2+H\big] - (Fr-Fr_{01})^2q_1^{-1} - \big[2+(Fr-Fr_{01})^2+2\rho H\big]q_1 + q_1^2 \\ \qquad -(Fr-Fr_{02})^2\rho Hq_2^{-1} - \rho H\big[(Fr-Fr_{02})^2+2(1+H)-2q_1\big]q_2 + \rho H^2q_2^2. \end{cases} \quad (10)$$

A suitable constant has been added to $\mathcal{H}_d$ in order to assure that both at-rest and at infinity ($\xi\to\infty$, $\mathbf{q},\mathbf{p}\to(1,1),(0,0)$) $\mathcal{H}_d\to 0$. We remark that $\mathbf{q}_c \equiv (1,1)$ represents a *critical point* of the dimensionless potential $\mathcal{V}_d(\mathbf{q},Fr)$, namely, $\mathcal{V}_d(\mathbf{q}_c,Fr)=0, \nabla_{\mathbf{q}}\mathcal{V}_d(\mathbf{q}_c,Fr)=\mathbf{0}$ as some easy calculations highlight. We point out that dimensionless parameters (9) do not define a *canonical transformation of variables*. For a given Fr, if $(\mathbf{q},\mathbf{p})$ are solutions of motion, then $\mathcal{H}_d(\mathbf{q},\mathbf{p},Fr)$ is a constant. Therefore, $\mathcal{H}_d(\mathbf{q},\mathbf{p},Fr)$ represents *a conserved quantity* but it cannot be considered a new Hamiltonian. It follows that the new differential system in the $\mathbf{q},\mathbf{p}$ variables,

$$\begin{cases} d\mathbf{q}/d\xi = \mathbf{F}_{\mathbf{q}}(\mathbf{q},\mathbf{p},Fr), \\ d\mathbf{p}/d\xi = \mathbf{F}_{\mathbf{p}}(\mathbf{q},\mathbf{p},Fr) \end{cases} \quad (11)$$

has to be obtained directly from Eq. (8) applying the change of variables (9). The explicit form of these equations is shown in the Appendix. It is worth noting that $\mathcal{H}_d$ and Eq. (11) are *Galileian invariant* under the transformation $Fr_{0i}\to Fr_{0i}+\delta$, $Fr\to Fr+\delta$ owing to they are function of Fr_{0i} and Fr [of the form $Fr-Fr_{0i}$ as shown by (10)]. As already discussed by la Forgia and Sciortino,[41] this allows to reduce the analysis to cases with one of the two layers at-rest (i.e., $Fr_{01}=0$, or $Fr_{02}=0$), without loss of generality.

To integrate first-order differential system (11), initial conditions $(\mathbf{q}(0),\mathbf{p}(0)) = (\mathbf{q}_0,\mathbf{p}_0)$ and parameters $(\rho,H,Fr_{01},Fr_{02},Fr)$ need to be defined. Following a similar approach as in la Forgia and Sciortino,[33,41] we look for the *limit* Froude number Fr_{Lim} for which the model admits soliton-solutions, namely for $|Fr|>|Fr_{Lim}|$ no *soliton solution* can exist. To this end, we calculate $\mathcal{H}_d$ in point $\mathbf{q}_m \equiv (q_{1m},q_{2m})$ of *maximum or minimum* of the soliton's profile, where $\mathbf{q}'=0\to\mathbf{p}=\mathbf{p}_m=\mathbf{0}$. Interestingly, by implementing this condition in (10) and imposing $\mathcal{H}_d(\mathbf{q}_m,\mathbf{0},Fr)=0$, we obtain

$$\begin{aligned} \hat{\mathcal{H}}_d(\mathbf{q}_m,Fr) \equiv\ & \big[(Fr-Fr_{01})^2-q_{1m}\big](q_{1m}-1)^2q_{2m} \\ & -\rho Hq_{1m}(q_{2m}-1)\big[(Fr-Fr_{02})^2 \\ & -(2+(Fr-Fr_{02})^2+H-2q_{1m})q_{2m}+Hq_{2m}^2\big] = 0. \end{aligned} \quad (12)$$

For *assigned values* of the *configuration parameters* (ρ,H,Fr_{01},Fr_{02}), Eq. (12) implicitly defines $Fr = Fr(q_{1m},q_{2m})$ as a function of (q_{1m},q_{2m}). To obtain the limit values $(\mathbf{q}_{Lim},Fr_{Lim}) \equiv (q_{1Lim},q_{2Lim},Fr_{Lim})$, two conditions are added to (12), in order to impose the stationarity of $Fr(q_{1m},q_{2m})$ with respect to (q_{1m},q_{2m}): $\partial Fr(q_{1m},q_{2m})/\partial q_{im}\big|_{\mathbf{q}_m=\mathbf{q}_{Lim}} = 0$.[41] By using the implicit differentiation, it follows:

$$\begin{cases} \partial\hat{\mathcal{H}}_d(\mathbf{q}_m,Fr_{Lim})/\partial q_{1m}\big|_{\mathbf{q}_m=\mathbf{q}_{Lim}} = 0, \\ \partial\hat{\mathcal{H}}_d(\mathbf{q}_m,Fr_{Lim})/\partial q_{2m}\big|_{\mathbf{q}_m=\mathbf{q}_{Lim}} = 0, \end{cases} \quad (13)$$

where $Fr_{Lim} \equiv Fr(q_{1Lim},q_{2Lim})$.

The three real unknowns $(q_{1Lim}, q_{2Lim}, Fr_{Lim})$ must satisfy suitable constraints in order to assure physical solutions: (i) the layers' thickness must be a positive real number, i.e., $q_{1Lim} > 0 \wedge q_{2Lim} > 0$; (ii) the layers' thickness displacements $\eta_1 - h_1$ and $\eta_2 - h_2$ have to be *out of phase*, i.e., $(\eta_1 - h_1)(\eta_2 - h_2) < 0$ [see (1)]. In dimensionless form, the second condition can be written as $(q_1 - 1)(q_2 - 1) < 0$. In conclusion, the limit dimensionless amplitudes and celerity $(q_{1Lim}, q_{2Lim}, Fr_{Lim})$ must fulfill the following polynomials system of three equations, with constraints,

$$\begin{cases} \hat{\mathcal{H}}_d(\mathbf{q}_{Lim}, Fr_{Lim}) = 0, \\ \partial\hat{\mathcal{H}}_d(\mathbf{q}_{Lim}, Fr_{Lim})/\partial q_{1Lim} = 0, \\ \partial\hat{\mathcal{H}}_d(\mathbf{q}_{Lim}, Fr_{Lim})/\partial q_{2Lim} = 0, \\ q_{1Lim} > 0 \wedge q_{2Lim} > 0 \wedge (q_{1Lim} - 1)(q_{2Lim} - 1) < 0. \end{cases} \tag{14}$$

where we denote with the symbols $\wedge, \vee$, respectively, "and," "or."

For assigned $(\rho, H, Fr_{01}, Fr_{02})$, many numerical tests confirmed that only two set of solutions of Eq. (14) exist: $(q_{1Lim}^{min,max}, q_{2Lim}^{min,max}, Fr_{Lim}^{min,max})$. They are related to *downstream-propagating* and *upstream-propagating* solitons, respectively.[41] In particular, when $Fr_{01} = Fr_{02} = 0$ these solutions have the form $(q_{1Lim}, q_{2Lim}, \pm Fr_{Lim})$, i.e., two equal solitons propagating with opposite celerities.

C. Dispersion relation and limit of the background shear current velocities

For the considered free-surface two-layer fluid system, we obtain the dispersion relation by defining the following *normal modes* $(i = 1, 2)$:

$$\begin{cases} \eta_i = h_i + \varepsilon_i h_1 \exp[Ik(x - \lambda t)], \\ u_i = u_{0i} + \varepsilon_{i+2}\sqrt{gh_1}\exp[Ik(x - \lambda t)], \end{cases} \tag{15}$$

where $I \equiv \sqrt{-1}$, and ε_j (with $j = 1, 2, 3, 4$) are small dimensionless parameters ($|\varepsilon_j| \ll 1$), λ is the wave celerity associated with the *normal mode* and k represents the related wave number. By substituting these normal modes in Eq. (2), and linearizing with respect to ε_j, a homogeneous linear system of four equations in the unknowns ε_j is derived. We impose that the determinant of the coefficient matrix is zero, and we implicitly obtain the dispersion relation as solution of a *fourth degree equation*. Introduced the dimensionless variables $\tilde{F}r \equiv \frac{\lambda}{\sqrt{gh_1}}$ and $K \equiv kh_1$, for a *long-wave* (i.e., for $K \to 0$), the *fourth degree equation* can be written as

$$\begin{aligned} &\left[(\tilde{F}r - Fr_{01})^2 - 1\right]\left[(\tilde{F}r - Fr_{02})^2 - H\right] - \rho H \\ &= \tilde{F}r^4 - 2(Fr_{01} + Fr_{02})\tilde{F}r^3 \\ &\quad + (Fr_{01}^2 + 4Fr_{01}Fr_{02} + Fr_{02}^2 - H - 1)\tilde{F}r^2 \\ &\quad - 2\left[Fr_{02}(Fr_{01}Fr_{02} + Fr_{01}^2 - 1) - HFr_{01}\right]\tilde{F}r \\ &\quad + (Fr_{01}^2 - 1)(Fr_{02}^2 - H) - \rho H = 0. \end{aligned} \tag{16}$$

Suitable values of parameters $(\rho, H, Fr_{01}, Fr_{02})$ assure that Eq. (16) admits *four real solutions* $\tilde{F}r$ (namely, *normal modes are stable*): $[\tilde{F}r^{(g_1)} \le \tilde{F}r^{(s_1)} \le \tilde{F}r^{(s_2)} \le \tilde{F}r^{(g_2)}]$. The two smallest in magnitude $[\tilde{F}r^{(s_1)} \le \tilde{F}r^{(s_2)}]$ represent the dimensionless celerities of the *baroclinic modes*, while the two largest in magnitude $[\tilde{F}r^{(g_1)} \le \tilde{F}r^{(g_2)}]$ provide the dimensionless celerities of the *barotropic modes*.[32] When $Fr_{01} = Fr_{02} = 0 \Rightarrow \tilde{F}r^{(s_{1,2})} = \pm\tilde{F}r^{(s)}$, $\tilde{F}r^{(g_{1,2})} = \pm\tilde{F}r^{(g)}$. We are not able to prove rigorously that soliton solutions can arise from numerical integration of differential system (11) only if the Froude Fr number satisfy the constraint,

$$Fr_{Lim}^{min} \le Fr \le \tilde{F}r^{(s_1)} \vee \tilde{F}r^{(s_2)} \le Fr \le Fr_{Lim}^{max}, \tag{17}$$

and to the author's knowledge, this problem is yet unsolved. However, a large number of numerical tests confirm this assumption, from a numerical point of view, at least. Moreover, these constraints are in agreement with Barros and Gavrilyuk,[34] Barros, Gavrilyuk, and Teshukov[35] for the case $Fr_{01} = Fr_{02} = 0$. It is anyway reasonable to consider dimensionless velocities $[\tilde{F}r^{(s_1)}, \tilde{F}r^{(s_2)}]$ as representatives for ISWs since *baroclinic* modes are always out of phase[32] just as interfacial and free-surface displacements appear for ISWs, in the absence of background shearing currents. Consistent with the hypothesis of infinitesimal $|\varepsilon_j|$, we observe that $[\tilde{F}r^{(s_1)}, \tilde{F}r^{(s_2)}]$ are the dimensionless celerities assumed by the *hidden-solitons*,[41] i.e., the ones traveling with $q_{amp1} = 0$ and $q_{amp2} = 0$.

The nature of the roots of Eq. (16) represents a fundamental issue. As highlighted by la Forgia and Sciortino[41] for the rigid-lid framework, this problem has relevant importance if one would obtain the *limit values* for the dimensionless velocities Fr_{01}, Fr_{02} composing the shearing current. This is immediate for $Fr_{01} = Fr_{02} = 0$, since Eq. (16) becomes *biquadratic* under these conditions (as shown in Refs. 34 and 35). Nevertheless, Wolfram Mathematica allowed us also to obtain analytic solutions for the general case $Fr_{01}, Fr_{02} \neq 0$, although the final output consists in a very complex function $\Delta Fr_0(H, \rho)$. For each assigned couple (H, ρ), this function defines the constraint $|Fr_{01} - Fr_{02}| \le \Delta Fr_0(H, \rho)$ associated with the shear dimensionless velocities Fr_{01}, Fr_{02}, which assure that all the roots of Eq. (16) are real and, consequently, that *normal modes are stable*. In conclusion, all scenarios in the *five-dimension* parametric space $(\rho, H, Fr_{01}, Fr_{02}, Fr)$ for which integration of system (11) provides soliton solutions, have to satisfy the following constraints:

$$\begin{cases} |Fr_{01} - Fr_{02}| \le \Delta Fr_0(H, \rho), \\ Fr_{Lim}^{min} \le Fr \le \tilde{F}r^{(s_1)} \vee \tilde{F}r^{(s_2)} \le Fr \le Fr_{Lim}^{max}. \end{cases} \tag{18}$$

Suitable initial conditions $(\mathbf{q}(0), \mathbf{p}(0)) = (\mathbf{q}_0, \mathbf{p}_0)$ should be imposed in order to assure the possible existence of homoclinic orbits (soliton solutions), as discussed by Barros and Gavrilyuk,[34] Barros, Gavrilyuk, and Teshukov.[35] We remark that all the four quantities $(Fr_{Lim}^{min}, \tilde{F}r^{(s_1)}, \tilde{F}r^{(s_2)}, Fr_{Lim}^{max})$ are function of $(\rho, H, Fr_{01}, Fr_{02})$.

III. RESULTS

To analyze the evolution of interfacial ISWs main features in the presence of a background shear current, we adopt the *HFS-ML* model for differently stratified two-layers fluid systems with a free surface. We set the density ratio $\rho = 0.99$ in order to schematize with a two-layer stratification the oceanic conditions.[34]

In the absence of background velocities (i.e., for $u_{01} = u_{02} = 0$), we examine soliton solutions predicted by the *HFS-ML* model for both elevation- and depression-type solitons, by setting the ratio of the layers thickness for the undisturbed stratification to $H < 1$ and $H > 1$, respectively. To investigate the role played by the free surface in

affecting solitons main features we follow a similar analysis as in la Forgia and Sciortino,[41] but removing the rigid-lid assumption. We then consider ISWs of elevation ($q_{amp1,0} = a_0/h_1 > 0$) for $H = \chi$ and ISWs of depression ($q_{amp1,0} < 0$) for $H = 1/\chi$, with the stratification parameter $\chi = 2, 3, 4, 10$ (Table I). We observe that χ represents a measure of the fluid system asymmetry with respect to the condition characterized by the same thickness for the two layers (i.e., $\chi = 1$ for $h_1 = h_2$). This allowed us to analyze two groups of stratifications for each soliton-type, characterized by the same reciprocal values of H considered by la Forgia and Sciortino.[41] Our first effort was to define a suitable criterion for properly comparing theoretical predictions derived by such different mathematical approaches (i.e., *HFS-ML* and *MCC-ML* formulations). Both models provide limit values for the soliton Froude number, although for given $(\rho, H, Fr_{01}, Fr_{02})$, they assumed different values. Thus, we define as comparable two ISWs if the associated Froude numbers assume the same normalized distance $0 \le r_{Fr} \le 1$ from the corresponding endpoints $\tilde{F}r^{(s_i)}$ derived from each theoretical model (Table I). By estimating r_{Fr} for cases considered by la Forgia and Sciortino,[41] we obtain the associated soliton Froude number Fr for the *HFS-ML* model as

$$\begin{cases} Fr = \tilde{F}r^{(s_1)} + r_{Fr}(Fr_{Lim}^{min} - \tilde{F}r^{(s_1)}), & for\ \ Fr_0 < 0, \\ Fr = \tilde{F}r^{(s_2)} + r_{Fr}(Fr_{Lim}^{max} - \tilde{F}r^{(s_2)}), & for\ \ Fr_0 > 0. \end{cases} \tag{19}$$

We remark that when $r_{Fr} = 1$, soliton Froude number corresponds to Fr_{Lim}^{min} or Fr_{Lim}^{max}, for $Fr_0 < 0$ and $Fr_0 > 0$, respectively. The condition $r_{Fr} = 0$ characterizes, instead, solitons with dimensionless celerity equal to $\tilde{F}r^{(s_j)}$ (with $j = 1$ for $Fr_0 < 0$ and $j = 2$ for $Fr_0 > 0$). This condition corresponds to the hidden-soliton configuration analyzed by la Forgia and Sciortino.[41]

For each case, we derive both a downstream and an upstream-propagating soliton. For background layers at-rest, the *HFS-ML* model predicts solitons with identical geometrical features, but propagating with Froude numbers that are equal in magnitude but opposite in sign. We impose a shear current acting at the background layers, by tuning the Froude number of one of the two layers (e.g., $Fr_{01} = 0$ and $Fr_{02} \neq 0$). Following the same criterion adopted by la Forgia and Sciortino,[41] considered the reverse layers name notation they adopted, we define as *downstream-propagating* ISWs:

- solitons traveling rightward for $Fr_{0i} = 0$, and interacting with a background shear characterized by $(Fr_{01} - Fr_{02}) \ge 0$;
- solitons traveling leftward for $Fr_{0i} = 0$, and interacting with a background shear characterized by $(Fr_{01} - Fr_{02}) \le 0$.

Moreover, we refer to *upstream-propagating* ISWs for

- solitons traveling rightward for $Fr_{0i} = 0$, and interacting with a background shear characterized by $(Fr_{01} - Fr_{02}) \le 0$;
- solitons traveling leftward for $Fr_{0i} = 0$, and interacting with a background shear characterized by $(Fr_{01} - Fr_{02}) \ge 0$.

We present herein the main soliton features derived by the *HFS-ML* model and we compare our results with those derived by the rigid-lid model.

A. Interfacial and surface profiles

In the absence of background velocities ($u_{01} = u_{02} = 0$), a downstream-propagating soliton with $q_{amp1,0} > 0$ induces positive (negative) fluid velocities in the lower (upper) layer ($u_{s1} > 0, u_{s2} < 0$).[38] For case 5 (Table I), the *HFS-ML* model predicts an interfacial profile [black solid line in Fig. 2(d)] which is in phase opposition with the associated free-surface dimensionless thickness $q_{amp,2} < 0$ [black solid line in Fig. 2(b)].

To investigate the solitons strain behavior induced by varying background shear currents, we increase the ratio between the ambient Froude number and the corresponding maximum magnitude provided by the theoretical model ($Fr_{02}/Fr_{02,max}$). In agreement with Stastna and Lamb[38] and la Forgia and Sciortino,[41] when the background fluid velocities assume the same direction of those induced by the ISW (i.e., $u_{b2} < 0$ and $u_{s2} < 0$) both the interfacial displacement and the free-surface profile are observed to broaden [Fig. 2(b)]. For even larger Fr_{02}, the interfacial wavelength continues to increase and its amplitude to reduce, up to reach the critical condition $q_{amp,1} = 0$ (the *hidden-soliton* condition[41]). Interestingly, associated with the absence of an interfacial displacement also the free surface presents a flat configuration (i.e., $q_{amp,2} = 0$), while the wave celerity assumes a finite value [see dashed lines in Figs. 2(c) and 2(d)]. In particular, for this configuration, the solitons assume a celerity equal to $\tilde{F}r^{(s_1)}$ or

TABLE I. List of the analyzed cases for different undisturbed stratified systems $H = h_2/h_1$. For solitons solution derived by the rigid-lid model, the magnitude of the Froude number $|Fr_0| = |c_0/\sqrt{gh_1}|$ and the normalized amplitude $q_{amp,0}$ are reported. The corresponding quantities predicted by the *HFS-ML* model (i.e., $|Fr_0|$ and $q_{amp1,0} = a_0/h_1$, respectively) and the associated free-surface maximum dimensionless thickness ($q_{amp2,0}$) are also shown. The normalized distance $r_{Fr,0}$ between Fr_0 and the endpoints $\tilde{F}r^{(s_i)}$ assumes the same value for both theoretical models.

				MCC-ML		HFS-ML		
Case	Soliton type	H	r_{Fr0}	$\lvert Fr_0\rvert(10^{-2})$	$q_{amp,0}$	$\lvert Fr_0\rvert(10^{-2})$	$q_{amp1,0}$	$q_{amp2,0}(10^{-3})$
1	Depression	1/10	0.968	5.187	−0.359	5.184	−0.359	1.30
2	Depression	1/4	0.964	5.564	−0.299	5.560	−0.299	1.20
3	Depression	1/3	0.963	5.759	−0.265	5.748	−0.266	1.10
4	Depression	1/2	0.961	6.126	−0.198	6.120	−0.199	0.92
5	Elevation	2	0.961	8.662	0.403	8.648	0.397	−2.10
6	Elevation	3	0.963	9.974	0.804	9.955	0.794	−4.10
7	Elevation	4	0.964	11.13	1.205	11.10	1.192	−6.10
8	Elevation	10	0.968	16.40	3.611	16.36	3.578	−17.3

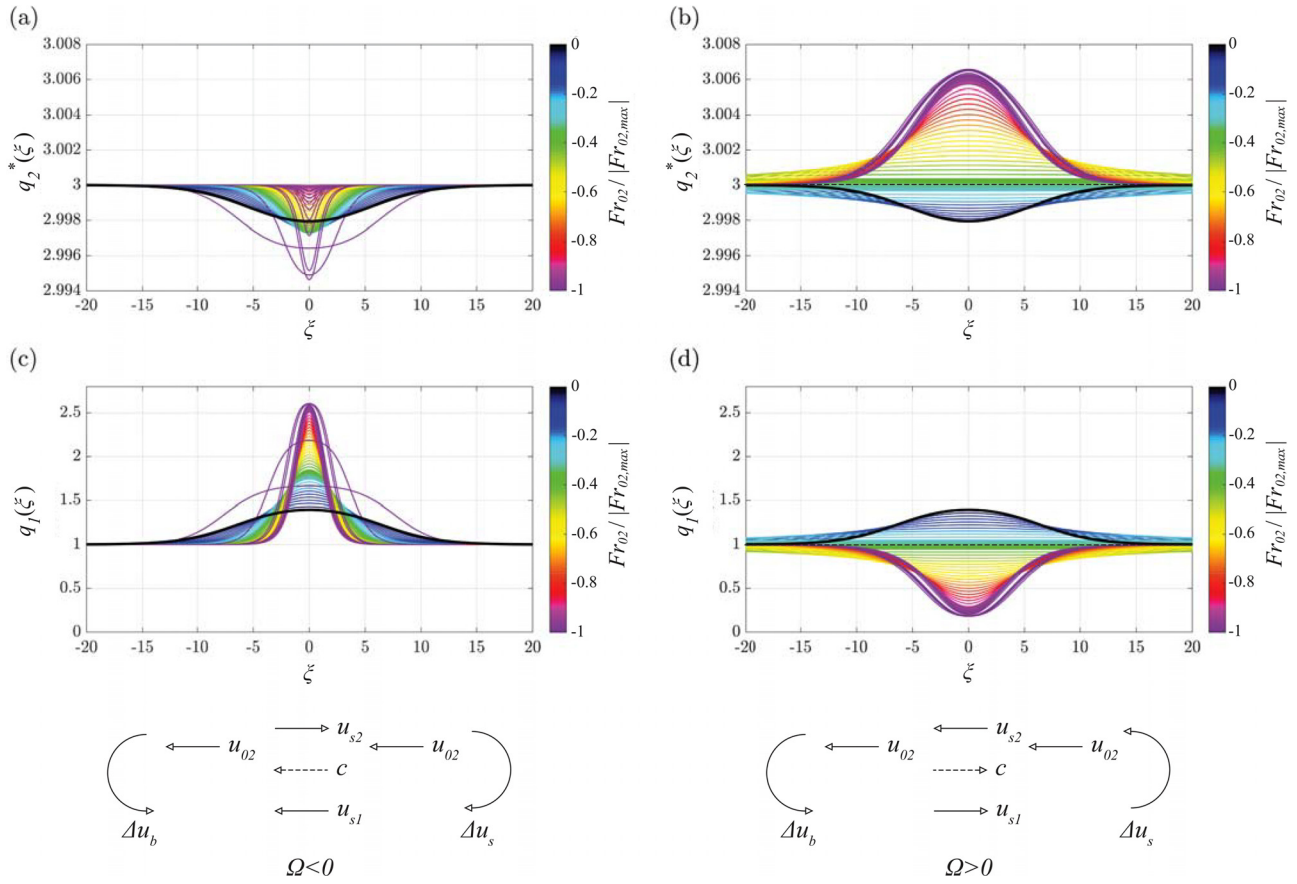

FIG. 2. Case 5: ISW of elevation for $H = 2$, $\rho = 0.99$. [(a) and (c)] Upstream-propagating and [(b) and (d)] downstream-propagating solitons. Evolution of [(a) and (b)] the dimensionless surface levels $q_2^* = q_1(\xi) + Hq_2(\xi)$ and [(c) and (d)] the dimensionless interfacial profiles $q_1(\xi)$ for changing $Fr_{02}/|Fr_{02,max}|$. Colors refer to the amount of shear current acting at the background with respect to the module of the limit value provided by the theoretical model. Arrows indicate directions associated with the ISW celerity (c), the soliton-induced velocities [$u_{s1} = u_{s1}(x)$, $u_{s2} = u_{s2}(x)$] and the background asymptotic velocity (u_{02}). The corresponding induced pseudovorticities (Δu_s, Δu_b) and the system deformation parameter Ω are reported.

$\tilde{Fr}^{(s_2)}$, obtained from the dispersion relation for waves traveling with infinitesimal amplitudes [Eq. 19)]. For this configuration also the propagating velocity-field induced by the soliton is zero and the fluid velocities correspond to the ones acting at the background $u_i = u_{0i}$ for $h_i = \eta_i$ [see Eq. (3)]. The *hidden-soliton* configuration represents a critical condition of incipient conversion of polarity for both the interfacial and the free-surface profiles. An even small increase in Fr_{02} leads the soliton to change the sign of both $q_{amp,1}$ and $q_{amp,2}$, which become negative and positive, respectively [Fig. 2(b)]. For larger Fr_{02}, the waves are then observed to steepen both the interfacial and the surface profiles, up to reach a final condition for $Fr_{02} = Fr_{02,max}$. A possible real field observation of ISWs converting polarity in response to background shearing currents may be the case of *hidden-soliton* condition recently captured by Xu *et al.*[49] in the South China Sea [see their Fig. 8(b)].

Case 5 soliton (Table I) shows a significantly different behavior as it propagates in the opposite direction [Figs. 2(a) and 2(c)]. For even larger background shear velocities acting at the background, the upstream-propagating soliton of elevation steepens its interface [Fig. 2(c)] while the free-surface profile is observed to broaden [Fig. 2(a)]. Thus, the free-surface strain behavior is opposite to the one observed for downstream-propagating solitons of elevation, after they invert the interfacial polarity. For increasing $|Fr_{02}|$, while the interfacial profile is observed to continuously steepen, the free surface reaches a flat configuration $q_{amp,2} = 0$ [Fig. 2(a)]. As for the downstream-propagating soliton, associate to this condition the fluid velocities correspond to the ones acting at the background $u_i = u_{0i}$. For very small increase in $|Fr_{02}|$, an abrupt change of the soliton strain behavior occurs: both the interfacial and the free-surface profiles starts broadening always preserving their phase opposition [see pink lines in Figs. 2(a) and 2(c)].

For zero background velocities (i.e., for $u_{01} = u_{02} = 0$), a downstream-propagating soliton of depression ($q_{amp,1} < 0$) induces negative (positive) fluid velocities in the lower (upper) layer ($u_2 > 0, u_1 < 0$).[40] For case 4 (Table I), the *HFS-ML* model predicts single-humped interfacial and surface profiles in phase opposition, with ($q_{amp,2} > 0$) [black solid line in Figs. 3(b) and 3(d)].

In agreement with Xu and Stastna[40] and la Forgia and Sciortino,[41] when $u_{b2} < 0$ and $u_{s2} > 0$, both interfacial and free-surface profiles are observed to continuously steepen until

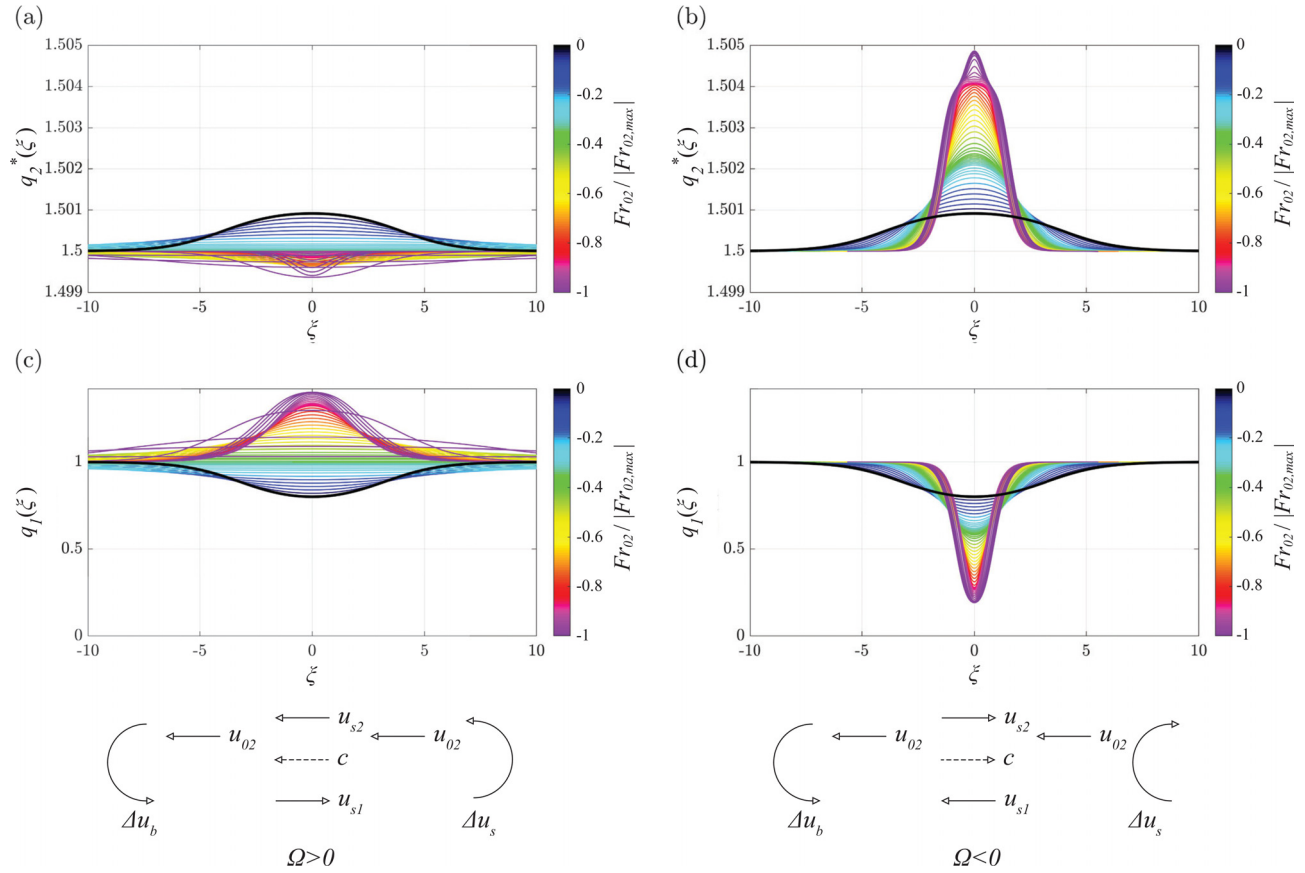

FIG. 3. Case 4: ISW of elevation for $H = 0.5$, $\rho = 0.99$. [(a) and (c)] Upstream-propagating and [(b) and (d)] downstream-propagating solitons. Evolution of [(a) and (b)] the dimensionless surface levels $q_2^* = q_1(\xi) + Hq_2(\xi)$ and [(c) and (d)] the dimensionless interfacial profiles $q_1(\xi)$ for changing $Fr_{02}/|Fr_{02,max}|$. Colors refer to the amount of shear current acting at the background with respect to the module of the limit value provided by the theoretical model. Arrows indicate directions associated with the ISW celerity (c), the soliton-induced velocities [$u_{s1} = u_{s1}(x)$, $u_{s2} = u_{s2}(x)$] and the background asymptotic velocity (u_{02}). The corresponding induced pseudovorticities (Δu_s, Δu_b) and the system deformation parameter Ω are reported.

$Fr_{02}/|Fr_{02,max}| = 1$. A very interesting behavior is observed at the free surface, which shows peculiar undulations, loosing the single-humped profile typically associated with internal solitons [$Fr_{02} > 0.7|Fr_{02,max}|$ in Fig. 3(b)]. Indeed, the ISWs *standard* free-surface profile is generally characterized by the presence of two inflection points and a single point of absolute maximum (minimum) for internal solitons of depression (elevation). Unlike the single-humped profiles of the interfacial displacements, for case 4, the shear current is able to induce deviations from the standard free-surface profile, which show four inflection points [Fig. 3(b)]. Although discussed more in detail in Sec. III C, we here point out that *nonstandard* free-surface profiles were never observed in the past under oceanic conditions, since they cannot develop for $\rho = 0.99$ in the absence of a shearing currents.

Downstream-propagating solitons of depression ($q_{amp1,0} < 0$), interacting with a background shear current with $Fr_{02} < 0$, show a broadening behavior of both the interfacial and surface profiles, as observed for solitons of elevation propagating downstream [Figs. 3(a) and 3(c)]. Then, for increasing magnitude of the ambient velocities they reach the *hidden-soliton* condition before inverting polarities of both $q_{amp,1}$ and $q_{amp,2}$.

Results inferred for ISWs with different initial polarities allow us to remark some general insights about solitons deformations induced by the background forcing, with specific reference to the evolution of the free surface. In agreement with Xu and Stastna,[40] the interfacial profile distortions can be described by the relation between two *pseudo* ambient-induced vorticities: the first induced by the background current, i.e., $\Delta u_b = (u_{02} - u_{01})/(h_1 + h_2)$, the second induced by the soliton, i.e., $\Delta u_s = (u_{s2,0} - u_{s1,0})/(h_1 + h_2)$. The latter considers layers velocities in the absence of background currents, at $x = 0$, i.e., in correspondence of the maximum interface displacement. We here define the *system deformation parameter* $\Omega = \Delta u_b/\Delta u_s$: when $\Omega > 0$, i.e., for $sign(\Delta u_b) = sign(\Delta u_s)$, for increasing background velocities, both depression and elevation type solitons show the broadening of the interfacial profiles, up to polarity inversion. Otherwise, for $\Omega < 0$, i.e., for $sign(\Delta u_b) \neq sign(\Delta u_s)$, both depression and elevation type solitons are observed to continuously steepen in response to increasing background forcing. Under oceanic conditions, a large number of numerical tests proved that Ω represents a significant parameter able to describe the expected interfacial profile distortions, since they are not affected by the stratification geometry (H). For most cases, the

free-surface deformations are observed to occur in accordance with those of the interfacial profiles. However, unlike the internal displacement, the behavior of the free-surface cannot be uniquely described by Ω. Indeed, for upstream-propagating solitons of elevation, associated with increasing shear, we observe the steepening of the interfacial profile and the broadening of the free surface. We can resume previous findings for solitons propagating through two-layer fluid systems forced by background shear currents as follows:

- for $\Omega > 0$ both the interfacial and the free-surface profiles broaden, inverting their undisturbed polarity. This is the case of downstream-propagating soliton of elevation ($q_{amp1,0} > 0$) and upstream-propagating soliton of depression ($q_{amp1,0} < 0$).
- for $\Omega < 0$ and $q_{amp1,0} < 0$ (i.e., for downstream-propagating soliton of depression), both the interfacial and the free-surface profile steepen, preserving their phase opposition;
- for $\Omega < 0$ and $q_{amp1,0} > 0$ (i.e., for upstream-propagating soliton of elevation), only the interfacial profile steepens, while the free-surface displacement broadens.

Moreover, although Cases 4 and 5 show that the phase opposition between the two displacements, this does not represent a general rule. Indeed, under particular circumstances, the free surface of upstream-propagating solitons of elevation appears in phase with the interfacial profile (see Sec. III C).

B. Free-surface and rigid-lid effects

To estimate the role of the top free surface in affecting ISWs features, we compare theoretical predictions provided by the *HFS-ML* model with those obtained by la Forgia and Sciortino,[41] under a rigid-lid assumption (Table I).

For differently stratified two-layer systems, we investigate the relation between solitons amplitude (q_{amp1}), normalized by their initial values ($q_{amp1,0}$, for $u_{01} = u_{02} = 0$), and the acting background, dimensionless velocity ratio ($Fr_{01}/|Fr_{01,max}|$). The corresponding quantities indicate the relative variation of the interfacial amplitude with respect to the undisturbed condition [i.e., the empty dot in Fig. 4(a), characterized by $Fr_{01} = 0$]. Arrows indicating the direction of the successive solitons stages for increasing $|Fr_{01}|$, refer to curves with the corresponding color. For all cases, the linear behavior of the different curves shows a direct proportionality between the ambient shear and the induced solitons amplitudes [Fig. 4(a)]. Consistent with the sign of the deformation parameter, for larger shear currents, downstream-propagating solitons of depression and upstream-propagating soliton of elevation linearly increase their amplitude [blue and red lines in Fig. 4(a), respectively]. A linear decrease in $q_{amp1}/q_{amp1,0}$, instead, is observed for fluid configurations characterized by $\Omega < 0$ [black and green lines in Fig. 4(a)]. The stratification geometry considerably affects the ISWs response: for larger H the curves slope increase: for a given $Fr_{01}/Fr_{01,max}$ solitons with larger H show a more pronounced variation of their amplitude, with respect to the associated undisturbed value. This leads solitons characterized by $\Omega > 0$ to invert their polarity for a relatively low background forcing, as they propagate through more asymmetric stratifications [see green and black dots in Fig. 4(a)].

To investigate how the presence of a free surface affects interfacial displacements, we analyze the difference between amplitudes predicted by the *HFS-ML* and *MCC-ML* models, i.e., q_{amp1} and q_{amp}, respectively [Fig. 4(b)]. We remark that quantity $(q_{amp1} - q_{amp})$ corresponds to

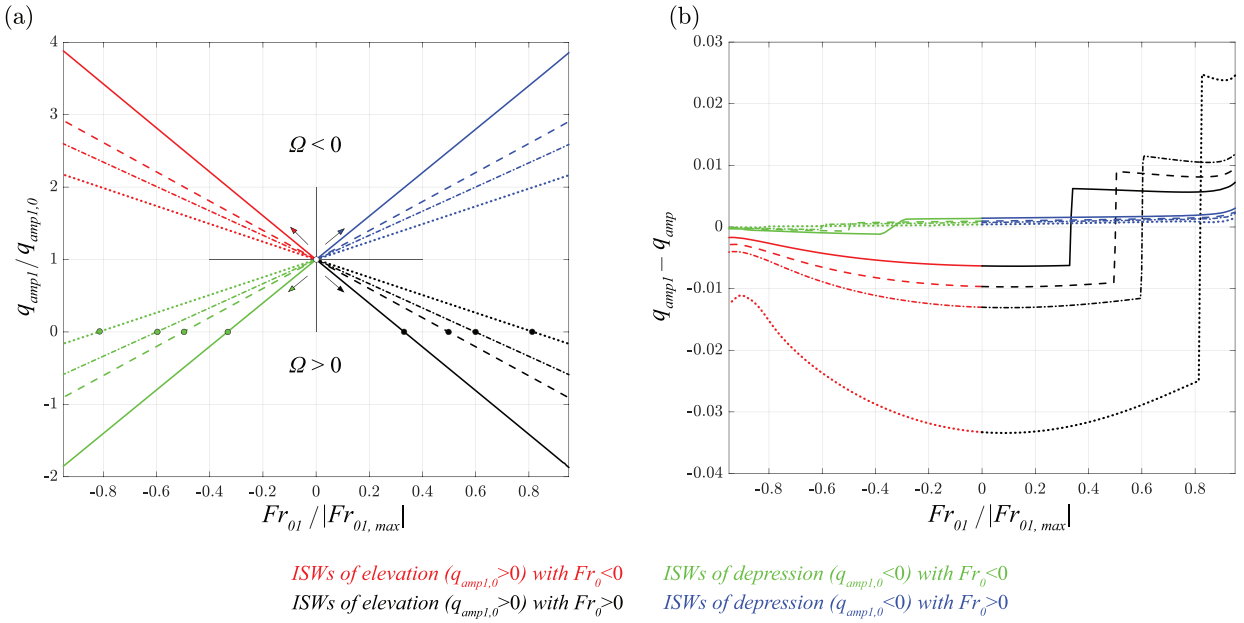

FIG. 4. (a) Relation between the soliton amplitudes q_{amp1} normalized by the initial value $q_{amp1,0}$ and the amount of shearing current acting at the background Fr_{01} with respect to the module of the limit value provided by the HFS-ML model ($Fr_{01,max}$). (b) Difference between the ISWs amplitudes predicted by the *HFS-ML* (q_{amp1}) and the one derived by the *MCC-ML* (q_{amp}) models, for changing amount of shearing current acting at the background. Arrows indicate the direction of the successive ISWs stages for increasing $|Fr_{01}|$. Four values of the stratification parameter are considered: $\chi = 2$ (solid lines), $\chi = 3$ (dashed lines), $\chi = 4$ (dashed–dotted lines), $\chi = 10$ (dotted lines).

the difference of the interfacial amplitudes with respect to the lower layer thickness [i.e., $(a_{HFS-ML} - a_{MCC-ML})/h_1$]. Results show that solitons of depression (elevation) always assume a relative larger (lower) amplitude when they are modeled with a free surface. The same behavior is observed also after solitons invert their polarity in response to increasing background velocities (discontinuities in black and green curves in Fig. 4(b) occur at the critical stages characterized by $q_{amp1} = 0$). To provide a physical explanation of these theoretical predictions, the role of buoyancy has to be considered. Indeed, solitons of depression induce positive buoyancy pressure in the upper layer, leading the free surface to assume a positive, upward displacement. The larger hydrostatic pressure loads acting at the interface are thus expected to generate a relatively larger interfacial displacement with respect to the one associated with a flat configuration of the free surface. Compared to the rigid-lid formulation, for the free-surface model an increase in buoyancy is then expected. For solitons of elevation, instead, negative buoyancy in the upper layer produces downward displacement of the free surface, and, consequently, relatively low hydrostatic pressure loads at the interface. Our results highlight that the rigid-lid model underestimates amplitudes for solitons of depression (approximately up to –0.3% under oceanic conditions), while the maximum interfacial displacement of ISWs of elevation overestimated (approximately up to +3.4% under oceanic conditions). For relatively low background forcing ($|Fr_{01}| < 0.2|Fr_{01,max}|$), the quantity $(q_{amp1} - q_{amp})$ remains roughly unvaried. However, for further increase in $|Fr_{01}|$, most cases show a lower difference between q_{amp1} and q_{amp} (e.g., see red curves for $0.2 < |Fr_{01}|/|Fr_{01,max}| < 0.9$). For increasing background velocities and dynamic pressures, we argue that interfacial displacements are expected to be less dependent on the hydrostatic pressure field, and, consequently, amplitudes provided by the two models are awaited to be more similar.

We also estimate the waves shape factor $r = a/\lambda_s$ in order to investigate changes in the steepness of the interfacial profiles [Fig. 5(a)]. Associated to the absence of background currents, relatively steeper waves are observed for more asymmetric two-layer fluid systems (i.e., the ones with a larger χ). A specular behavior characterizes downstream- and upstream-propagating solitons forced by shear currents. Consistent with the analyzed deformations of the wave profiles, within the range $-0.5 < Fr_{01}/|Fr_{01,max}| < 0.5$ a significant increase in r occurs for cases with $\Omega < 0$, while the wave steepness decreases up to zero for cases with $\Omega > 0$. For larger background shear amplitude of downstream-propagating soliton of depression (blue lines) and upstream-propagating soliton of elevation (red lines) further increase up to become slightly larger than three times the corresponding wavelengths (for $\chi = 10$). These waves are the one that shows the more significant difference in wave steepness with respect to prediction provided for the corresponding case by the rigid-lid model [Fig. 5(b)]. Unlike the interfacial strain behavior, variations in solitons celerity in response to background shearing currents, cannot be predicted by Ω and $q_{amp1,0}$. In agreement with the recent literature,[38,40,41] our cases show that, with respect to the initial, normalized wave phase speed Fr_0, downstream- and upstream-propagating solitons accelerate and decelerate, respectively, as they are forced by a background forcing. We remark that this evidence is valid for magnitudes of shear currents conveniently lower than $|Fr_{01,max}|$ [Fig. 6(a)].

In order to generalize these results, we performed a large number of numerical tests by varying both direction and magnitude of the background layers velocity (i.e., Fr_{01} and Fr_{02}), by imposing one of two layers at-rest. Taking into account the reference system defined in

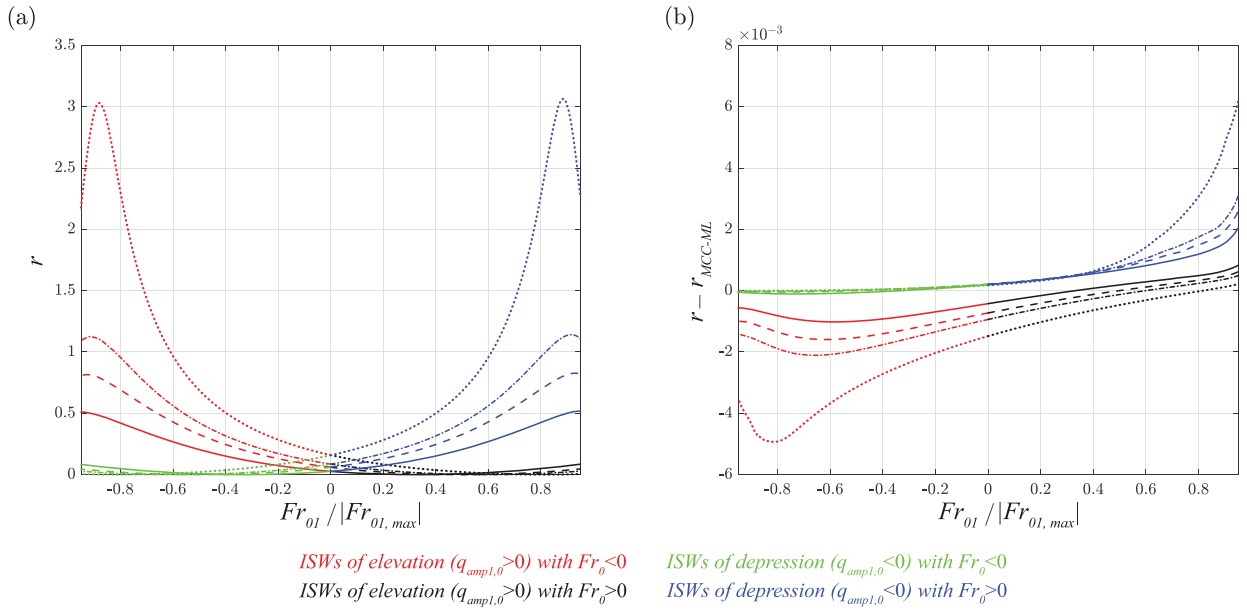

FIG. 5. (a) Relation between the soliton shape factor $r = a/\lambda_s$ and the amount of shearing current acting at the background Fr_{01} with respect to the module of the limit value provided by the *HFS-ML* model ($Fr_{01,max}$). (b) Difference between the soliton shape factor predicted by the *HFS-ML* (r) and the one derived by the *MCC-ML* (r_{MCC-ML}) models, for changing amount of shearing current acting at the background. Four values of the stratification parameter are considered: $\chi = 2$ (solid lines), $\chi = 3$ (dashed lines), $\chi = 4$ (dashed–dotted lines), $\chi = 10$ (dotted lines).

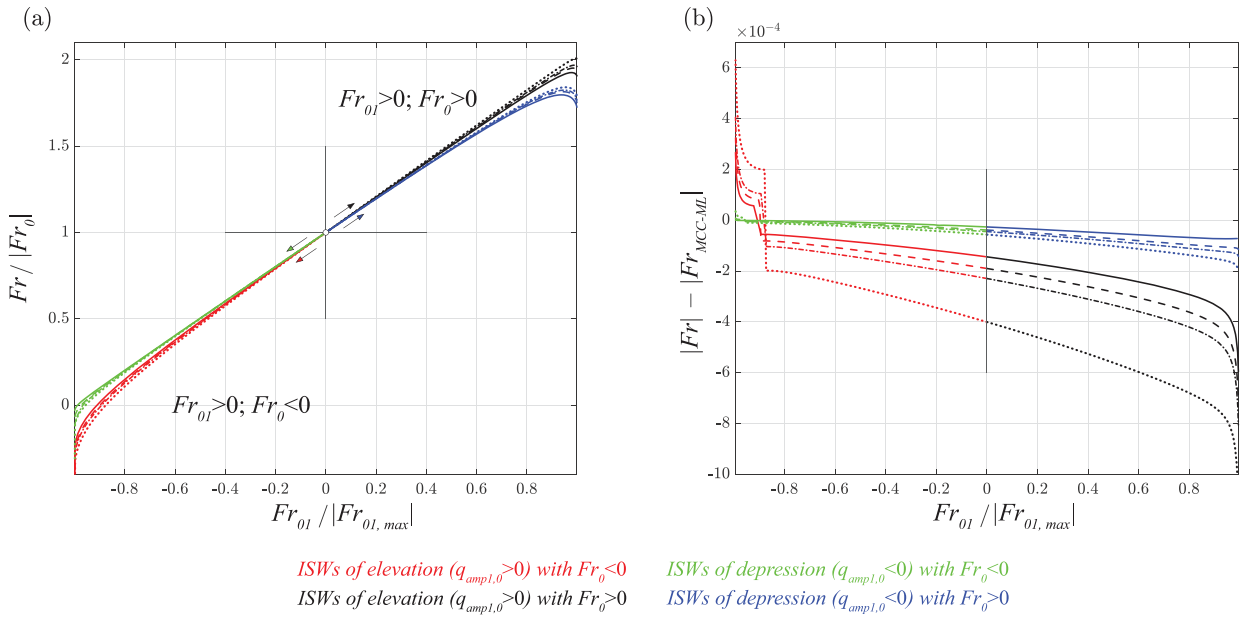

FIG. 6. (a) Relation between the soliton Froude number Fr normalized by the module of the initial value Fr_0 and the amount of shearing current acting at the background Fr_{01} with respect to the module of the limit value provided by the HFS-ML model ($Fr_{01,max}$). (b) Difference between the ISWs Froude number predicted by the *HFS-ML* ($|Fr|$) and the one derived by the *MCC-ML* ($|Fr_{MCC-ML}|$) models, for changing amount of shearing current acting at the background. Cases are described in the figure legend. Arrows indicate the direction of the successive ISWs stages for increasing $|Fr_{01}|$. Four values of the stratification parameter are considered: $\chi = 2$ (solid lines), $\chi = 3$ (dashed lines), $\chi = 4$ (dashed–dotted lines), $\chi = 10$ (dotted lines).

Fig. 1, we observe that changes of the undisturbed ISWs phase speed Fr_0 can be predicted by the sign of the background velocity. In particular, for $Fr_{0i} > 0$ (with $i = 1$ or $i = 2$) a positive variation of the soliton celerity occurs, such that if $Fr_0 > 0$ than $Fr > Fr_0$, while for $Fr_0 < 0$, Fr tends to zero, and an inversion of the direction of propagation may occur in response to larger shearing current. On the other end, when $Fr_{0i} < 0$ (with $i = 1$ or $i = 2$) a negative variation of the soliton celerity is observed.

As for the interfacial amplitudes, we investigate how the presence of a free surface affects soliton celerity in response to a background forcing. For this analysis, we compute the difference between magnitudes of ISWs Froude numbers predicted by the *HFS-ML* and *MCC-ML* models [i.e., $|Fr| - |Fr_{MCC-ML}|$, Fig. 6(b)]: it represents the difference in wave celerity predictions [i.e., $(c_{HFS-ML} - c_{MCC-ML})$] normalized by $\sqrt{gh_1}$. Consistent with previous studies,[32,33] in the absence of shear currents, the rigid-lid model overestimates the waves celerity [see Fig. 6(b) for $Fr_{01} = 0$]. This is all the more pronounced for solitons of elevation and for more asymmetric two-layer stratified systems. In the presence of a shear current characterized by $-0.8 < Fr_{01}/|Fr_{01,max}| < 1$, the difference $|Fr| - |Fr_{MCC-ML}|$ appears significantly affected from the wave celerity: for larger wave speeds, the *HFS-ML* model predicts even lower celerities, compared to the *MCC-ML* model [Fig. 6(b)]. Interestingly, for upstream-propagating solitons, this trend undergoes an abrupt change after the solitons celerity becomes zero, and waves invert their original direction of propagation. Under these conditions, indeed, the rigid-lid model predictions provide relatively slower solitons.

C. Deviations from the standard free-surface profile

For density distributions similar to those observed in the real field ($\rho = 0.99$), numerical studies, laboratory experiments, and theoretical predictions performed with both layers at-rest, showed that ISW-induced surface displacements are composed of single hump-shaped profiles.[32,34] Results obtained from the *HFS-ML* model also confirm this occurrence both in the absence of a background shear ($u_{01} = u_{02} = 0$) and for equal background velocities (i.e., for $u_{01} = u_{02} \neq 0$). Indeed, a uniform current does not induce modifications of waves profile with respect to the undisturbed condition, but it can only affect their phase speed.[41]

In the presence of a shear background current, although interfacial profiles always preserve their single-humped shape, the associated free-surface displacement can show *nonstandard* configurations. This evidence is uniquely observed for cases characterized by $\Omega < 0$ (Fig. 7): the steepening of the interfacial profiles occurs in response to the opposite direction between the current-induced and the ISW-induced velocities [i.e., $u_{si}(\xi)$ and $u_{bi}(\xi)$, respectively]. For increasing $|Fr_{02}|$, both solitons of elevation [Figs. 7(a)–7(c)] and depression [Figs. 7(d) and 7(e)] show undulations of the free-surface profiles, which develop symmetrically with respect to vertical line passing soliton crest/trough. Based on theoretically predictions, two *nonstandard* free-surface profiles can be distinguished: (i) undulated profiles, which present more than two inflection points but a single maximum [e.g., Fig. 7(e) for $Fr_{02} \simeq -0.95$], and (ii) multihumped profiles, characterized by multiple relative maxima/minima [e.g., Fig. 7(e) for $Fr_{02} \simeq -0.8$].

For larger χ, i.e., for more asymmetric two-layers stratifications, these free-surface disturbances appear more pronounced and occur

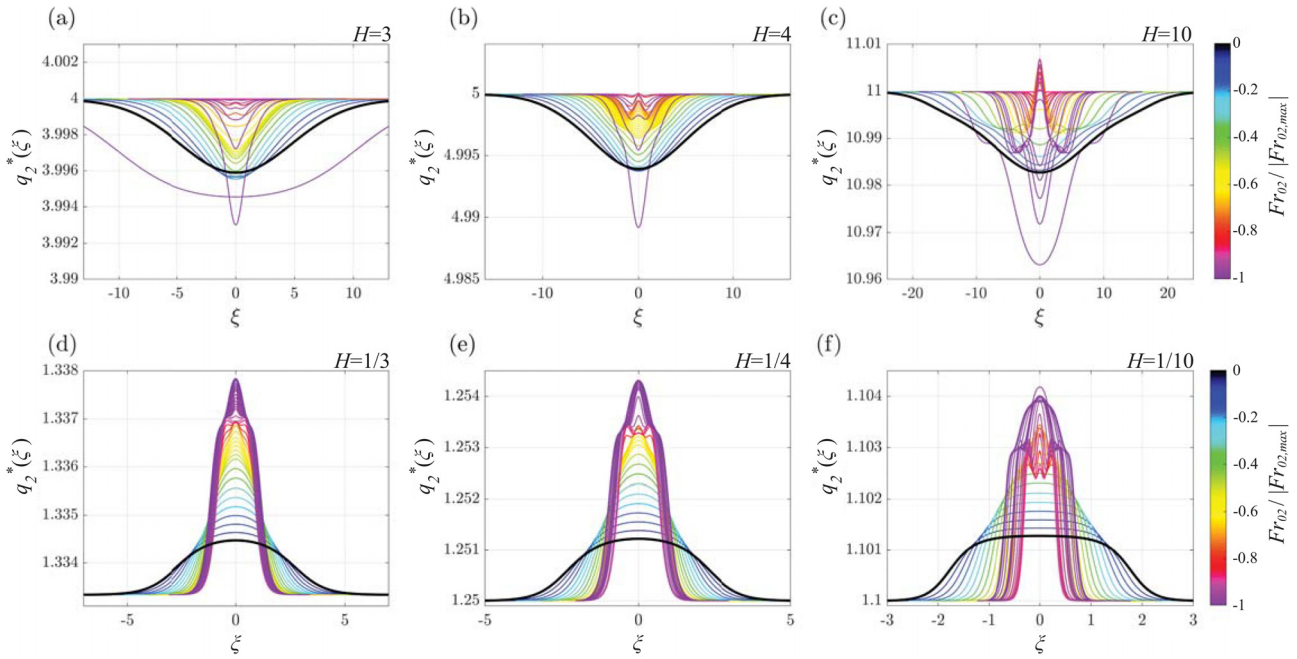

FIG. 7. Dimensionless surface levels $q_2^* = q_1(\xi) + Hq_2(\xi)$ for cases with $\Omega < 0$: [(a)–(c)] upstream-propagating soliton of elevation and [(d) and (e)] downstream-propagating solitons of depression, for changing $Fr_{02}/|Fr_{02,max}|$. (a) case 6; (b) case 7; (c) case 8; (d) case 3; (e) Case: 2; (f) case 1.

for relatively low background velocities. In response to an increasing background velocities, free-surface displacements are observed to develop differently depending on the undisturbed interfacial polarity. Associated to the steepening of the interfacial profiles, solitons of depression show a non-uniform increase in the free-surface displacement along the ξ-axis. For larger Fr_{02}, indeed, the lateral edges are observed to assume higher elevations compared to central regions, closer to $\xi = 0$ [e.g., see Fig. 7(e) for $Fr_{02}/|Fr_{02,max}| \simeq -0.8$]. In response to further increase in $|Fr_{02}|$, we observe a significant raising of the free-surface displacements around $\xi = 0$, such that a clearly visible bump characterizes the final surface profile (for $Fr_{02} \to Fr_{02,max}$). Solitons of elevation behave differently: they evolve by lowering the lateral edges of the free-surface profile [Figs. 7(a)–7(c)]. In correspondence of the maximum interfacial displacement, instead, the free surface shows a relative larger displacement. Surprisingly, for solitons characterized by the largest χ (e.g., case 8), this allows the free surface to lose locally the typical phase opposition with respect to the associated interfacial displacement and to assume positive ζ_2 values [Fig. 7(c)].

Our results show that shear currents flowing in opposite direction with respect to the soliton-induced velocities are able to excite free-surface disturbances, leading the standard soliton profile to assume undulated or multihumped configurations. Considered their symmetric development with respect to the maximum interfacial displacement, we argue that these surface manifestations cannot be considered as short-surface waves generated by a resonance mechanism between the interface and the free surface, as the ones observed and discussed by Kodaira *et al.*[32] Rather, they are presumably caused by the non-hydrostatic pressure field associated with the internal wave. We remark, indeed, that free-surface disturbances are observed only for solitons that steepen their interfacial profile in response to increasing background shears. Thus, centrifugal effects induced by the non-negligible curvature of the interface (and, consequently, of the streamlines) are expected to induce significant dynamic stresses at the free surface.

Our assumptions could be rigorously confirmed by estimating the total pressure field in the plane (x, z). However, the theoretical formulation considered in the present study is developed in a shallow water framework, and only depth-averaged quantities for each layer can be derived. Hence, the pressure distribution along the z-axis is unknown. To investigate the role of dynamic forces in affecting the surface profiles, from the *HFS-ML* model equations, we isolate the term

$$\frac{\partial P_{NH}}{\partial x} = -\rho_2 \frac{\partial}{\partial x}\left(\frac{1}{2}\eta_2^2 G_2 - \eta_2 D_2^2 \eta_1\right), \tag{20}$$

which can be numerically integrated to derive the dimensionless non-hydrostatic pressure acting at the interface $P_{NH}(x)$ [e.g., see Figs. 8(c) and 8(f)]. For each case, we also calculate the buoyancy-induced surface displacement $1 + H - \zeta_1(1-\rho)/h_1$ [e.g., see thin lines in Figs. 8(b) and 8(e)], which represents the free-surface profile expected if uniquely hydrostatic contributions were considered (i.e., buoyancy). Thus, the comparison with the theoretical–predicted free-surface profile [solid line in Figs. 8(b) and 8(e)] allows us to qualitatively estimate the dynamic pressure effects in reshaping the surface profiles. We find that the distribution of nonhydrostatic pressure acting at the interface $[\tilde{P}_{NH}(\xi)]$ resembles the dynamic pressure contribution expected at the free surface, suggesting a strong relation between the nonhydrostatic forces and the short-surface disturbances. This is primarily confirmed by the correspondence of the inflection points between the $q_1(\xi) + Hq_2(\xi)$ and $\tilde{P}_{NH}(\xi)$ (Fig. 8). This suggests that nonhydrostatic pressures excited by the steepening of the interfacial profiles represent

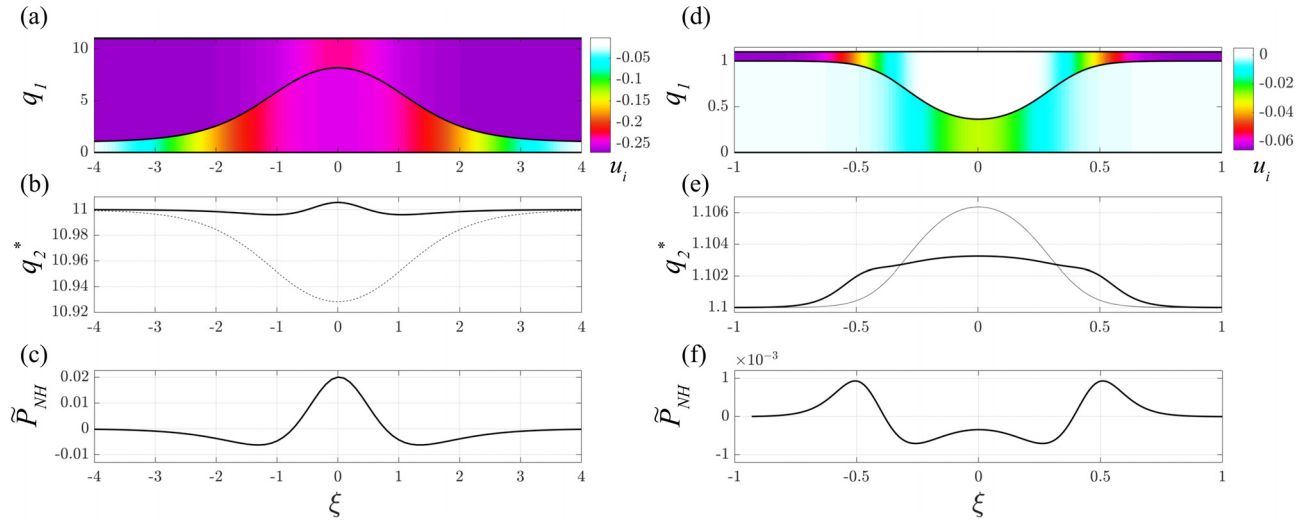

FIG. 8. Interfacial and free surface features of [(a)–(d)] case 8 upstream-propagating soliton of elevation in the presence of a background shear current $Fr_{02}/|Fr_{02,max}| = -0.81$. and [(e) and (f)] case 1 downstream-propagating soliton of depression in the presence of a background shear current $Fr_{02}/|Fr_{02,max}| = -0.63$. [(a) and (e)] horizontal velocity fields $u(\xi)$; [(b) and (e)] dimensionless free-surface profile [$q_2^* = q_1(\xi) + Hq_2(\xi)$, solid lines] and buoyancy-induced surface displacement (thin lines); [(c) and (f)] nonhydrostatic pressure $\tilde{P}_{NH}$ obtained by integrating Eq. (20).

the main cause of short disturbances experienced by the free-surface profiles. This is in full agreement with other evidence resulting from theoretical predictions. Indeed, associated with larger χ, the free-surface disturbances are more pronounced and occur for relative lower magnitude of the background shear current (Fig. 7). This results to consistent with the more pronounced steepening (i.e., larger nonhydrostatic pressures) observed for more asymmetric stratified systems [Fig. 5(a)]. Moreover, it is not surprising that any surface disturbances are observed for cases with $\Omega < 0$, as the interfacial profiles broaden in response to increasing shear currents [e.g., see Fig. 3(a) and 3(c)].

IV. DISCUSSION AND CONCLUSIONS

Following the Hamiltonian approach, we implement a mathematical formulation (the *HFS-ML* model) aimed at predicting interfacial solitons features as they propagate through a background shear current, in a two-layer stratified system with a free surface. A real field density configuration is properly set by imposing a density ratio between the two layers equal to 0.99. The ratio between the layers' thickness was instead varied in order to study both solitons of elevation and depression, under different stratified configurations.

For each case, we imposed a shear current, by introducing a background velocity for one of the two layers. In response to increasing background forcing, we found that changes in waves celerity, and deformations of both interfacial and surface profiles experienced by undisturbed solitons (i.e., for $Fr_{0i} = 0$), can be predicted by analyzing the sign assumed by three dimensionless parameters: the initial wave polarity ($q_{amp1,0}$), the deformation parameter (Ω) and the background velocity (Fr_{0i}). The latter allows to predict if the initial, undisturbed wave celerity will assume positive (for $Fr_{0i} > 0$) or negative (for $Fr_{0i} < 0$) variations. The evolution of solitons shape can be predicted by the signs assumed by $q_{amp1,0}$ and Ω. The deformation parameter is obtained as the ratio between the soliton- and the background-induced pseudo vorticities. For increasing background shears, if the induced pseudo-vorticities are concordant, both the interfacial and the free-surface profiles are observed to broaden, up to invert their initial polarity. For $\Omega < 0$, although the interfacial profiles always steepen, the free surface is observed to broaden or steepen depending on the initial wave polarity (for positive and negative $q_{amp1,0}$, respectively).

Our investigation showed that shear currents flowing against the soliton-induced velocities can lead solitons to lose the single-humped shape commonly observed at the free surface. Undulated and multi-humped free-surface profile appears as short-wave disturbances can develop in response to the interfacial profile steepening, which, in turn, enhances the non-hydrostatic pressure components. For solitons of elevations, this can leads the free surface to locally lose the typical phase opposition with respect to the associated interfacial displacement (i.e., $\zeta_1\zeta_2 > 0$). We remark, however, that for all cases, the product $(q_1 - 1)(q_2 - 1)$ is always negative.

By comparing our results with those obtained for the same cases by la Forgia and Sciortino[41] under rigid-lid conditions, it was possible to investigate how the presence of a free surface may affect soliton's main features. We found that the buoyancy-induced free-surface displacements cause solitons of depression (elevation) to assume a relative larger (lower) amplitude than the ones predicted by a rigid-lid model. For finite background velocities, differences between predictions provided by the two models are non-negligible for real field density distributions, characterized by lower layers thickness of about 10^2 m.[13] Indeed, our results show, that the presence of the free surface could lead the maximum interfacial displacements to be $\simeq$1 m larger and $\simeq$10 m lower for elevation- and depression-type solitons, respectively. Furthermore, also substantial changes in waves phase speed predictions raised from our analysis. For most cases, the rigid-lid assumption produces an overestimation of solitons celerities. Downstream-propagating interfacial waves predicted by of the *HFS-ML* model are slower than the one derived from the *MCC-ML* model, particularly for even more energetic background forcings (up to $\simeq$10 cm/s for solitons of elevation). Interestingly, upstream-propagating solitons showed an opposite behavior: as they invert their

direction of propagation, indeed, the rigid-lid model predictions provide relatively slower solitons. Although under oceanic conditions the rigid-lid assumption represents a good approximation, ISWs features may be substantially affected by the free surface, as they are forced by a background shear current. We point out that ISWs breaking, and the consequent induced mixing, is strongly affected also by small changes in solitons features.[19,22] Both the breaking mechanism and the wave energy, indeed, may significantly change in response to small variations of waves slopes, profiles, and celerity. Our results suggest that in the presence of shearing currents, a rigid-lid approach is suitable only for investigating the propagation of ISWs over a flat bottom. To model the ISWs breaking processes, instead, the presence of the free surface cannot be neglected. Indeed, more accurate estimations of the incident waves features are needed in order to characterize more realistic initial conditions before the waves shoaling.

APPENDIX: INITIAL CONDITIONS, DISPERSIVE NONLINEAR TERMS AND DIMENSIONLESS FORM OF THE HAMILTON'S EQUATIONS

1. Choice of initial conditions for the *HFS-ML* model

The choice of initial condition $(\mathbf{q}(0),\mathbf{p}(0))=(\mathbf{q}_0,\mathbf{p}_0)$ is a fundamental step if one would obtain soliton solutions from the differential system (11). To consider also the existence of multi-humped solitons, we follow the technique proposed by Barros and Gavrilyuk,[34] Barros, Gavrilyuk, and Teshukov.[35] It consists in linearizing Eq. (11) in the neighborhood of the critical point $(\mathbf{q}_c,\mathbf{0})=(1,1,0,0)$ in order to leave from a small neighborhood of the saddle point $\mathbf{q}_c\equiv(1,1)$ of the dimensionless potential $\mathcal{V}_d(\mathbf{q})$, and to remain as close as possible from the *true homoclinic orbit*.

For differential system (11), we thus derive the following linear solution:

$$(\mathbf{q}_l(\xi),\mathbf{p}_l(\xi))\equiv(\mathbf{q}_c,\mathbf{0})+\varepsilon(\delta\mathbf{q}(\xi),\delta\mathbf{p}(\xi)), \tag{A1}$$

where ε is a small, real parameter. We substitute Eq. (A1) in Eq. (11), and we linearize with respect to ε. By considering that $(\mathbf{q}_c,\mathbf{0})$ is a stationary solution of these equations, it follows:

$$d(\delta\mathbf{q}(\xi),\delta\mathbf{p}(\xi))^T/d\xi=\mathcal{A}(\delta\mathbf{q}(\xi),\delta\mathbf{p}(\xi))^T, \tag{A2}$$

where $\mathcal{A}=\mathcal{A}(\rho,H,Fr_{01},Fr_{02},Fr)$ is a 4×4 matrix defined in the Appendix and $(\bigcirc)^T$ the transpose operation. If constraints (18) are fulfilled, for all our numerical tests, this matrix shows two purely imaginary and two real and opposite eigenvalues.[34,35] Consequently, there will be only one positive eigenvalues Λ_+ with associate a *nonoscillating and nondecaying* solution of the linear differential equation (A2),

$$(\delta\mathbf{q}(\xi),\delta\mathbf{p}(\xi))=\mathbf{Y}\,\mathrm{Exp}(\Lambda_+\xi), \tag{A3}$$

where $\mathbf{Y}\equiv(y_{q_1},y_{q_2},y_{p_1},y_{p_2})$ is the associate eigenvector: $\mathcal{A}\mathbf{Y}^T=\Lambda_+\mathbf{Y}^T$.

In conclusion, $(\mathbf{q}_l(\xi),\mathbf{p}_l(\xi))=(\mathbf{q}_c,\mathbf{0})+\varepsilon\mathbf{Y}\,\mathrm{Exp}(\Lambda_+\xi)$ is a linearized solution of Eq. (11) in the neighborhood of the critical point $(\mathbf{q}_c,\mathbf{0})$, which is able to provide as initial conditions,

$$\begin{aligned}(\mathbf{q}(0),\mathbf{p}(0))&=(\mathbf{q}_l(0),\mathbf{p}_l(0))\\&=(\mathbf{q}_c,\mathbf{0})+\varepsilon\mathbf{Y}=(1+\varepsilon y_{q_1},1+\varepsilon y_{q_2},\varepsilon y_{p_1},\varepsilon y_{p_2}).\end{aligned} \tag{A4}$$

Initial condition in (A4) are those closest to the *true homoclinic orbit* (ε close to zero). Since $\mathrm{Exp}(\Lambda_+\xi)$ is an increasing function with respect to ξ ($\Lambda_+>0$), the sign of ε has to be taken into account in order to choose suitable small values. For depression-type solitons, it thus results: $q_1(0)<1\rightarrow\varepsilon y_{q_1}<0$ and $sign(\varepsilon)=-sign(y_{q_1})$; for elevation-type solitons, instead, $\varepsilon y_{q_1}>0$, then $sign(\varepsilon)=sign(y_{q_1})$.

2. Definition of dispersive nonlinear terms $disp_i$

$$\begin{cases}disp_1\equiv\dfrac{1}{\eta_1}\dfrac{\partial}{\partial x}\left(\dfrac{1}{3}\eta_1^3G_1\right)+\dfrac{\rho_2}{\rho_1}\dfrac{\partial}{\partial x}\left(\dfrac{1}{2}\eta_2^2G_2-\eta_2D_2^2\eta_1\right),\\ disp_2\equiv\dfrac{1}{\eta_2}\dfrac{\partial}{\partial x}\left(\dfrac{1}{3}\eta_2^3G_2-\dfrac{1}{2}\eta_2^2D_2^2\eta_1\right)+\left(\dfrac{1}{2}\eta_2G_2-D_2^2\eta_1\right)\dfrac{\partial\eta_1}{\partial x},\\ G_i\equiv\dfrac{\partial^2u_i}{\partial x\partial t}+u_i\dfrac{\partial^2u_i}{\partial x^2}-\left(\dfrac{\partial u_i}{\partial x}\right)^2=-\dfrac{1}{\eta_i}(D_i^2\eta_i),\\ i=1,2.\end{cases}$$

3. Hamilton's equations in the dimensionless form

$$\begin{cases}dq_1/d\xi=\dfrac{6q_1q_2(2p_1-3Hp_2\rho)}{4(Fr-Fr_{01})^2q_2+3(Fr-Fr_{02})^2Hq_1\rho},\\ dq_2/d\xi=\dfrac{6q_2\left[2(Fr-Fr_{01})^2p_2q_2-3(Fr-Fr_{02})^2q_1(p_1-2Hp_2\rho)\right]}{(Fr-Fr_{02})^2H\left[4(Fr-Fr_{01})^2q_2+3(Fr-Fr_{02})^2Hq_1\rho\right]},\\ dp_1/d\xi=-\{16(Fr-Fr_{01})^6q_2^2+24(Fr-Fr_{01})^4(Fr-Fr_{02})^2Hq_1q_2\rho+18(Fr-Fr_{02})^4H^2q_1^5\rho^2\\ \quad-8(Fr-Fr_{01})^2q_1^3q_2\left[3(Fr-Fr_{02})^2H\rho(2+(Fr-Fr_{01})^2+2H\rho)-2q_2(2(Fr-Fr_{01})^2+3(Fr-Fr_{02})^2H^2\rho^2)\right]\\ \quad-3(Fr-Fr_{02})^2Hq_1^4\rho\left[3(Fr-Fr_{02})^2H\rho(2+(Fr-Fr_{01})^2+2H\rho)-2q_2(8(Fr-Fr_{01})^2+3(Fr-Fr_{02})^2H^2\rho^2)\right]\\ \quad+(Fr-Fr_{01})^2q_1^2[9(Fr-Fr_{02})^4H^2\rho^2+4q_2^2[8(Fr-Fr_{01})^2Hq_2\rho-4(Fr-Fr_{01})^2(2+(Fr-Fr_{01})^2+2H\rho)\\ \quad+3(2p_1-3Hp_2\rho)^2]]\}/\{2q_1^2[4(Fr-Fr_{01})^2q_2+3(Fr-Fr_{02})^2Hq_1\rho]^2\},\\ dp_2/d\xi=\dfrac{1}{2H}\left[2+(Fr-Fr_{02})^2+2H-\dfrac{3p_2^2}{(Fr-Fr_{02})^2}-2q_1-\dfrac{(Fr-Fr_{02})^2}{q_2^2}-2Hq_2-\dfrac{9(Fr-Fr_{02})^2q_1^2(2p_1-3Hp_2\rho)^2}{\left[4(Fr-Fr_{01})^2q_2+3(Fr-Fr_{02})^2Hq_1\rho\right]^2}\right].\end{cases}$$

4. Definition of the matrix $\mathcal{A}$

$$\mathcal{A} \equiv \begin{pmatrix} 0 & 0 & \mathcal{A}_{1,3} & \mathcal{A}_{1,4} \\ 0 & 0 & \mathcal{A}_{2,3} & \mathcal{A}_{2,4} \\ \mathcal{A}_{3,1} & \mathcal{A}_{3,2} & 0 & 0 \\ \mathcal{A}_{4,1} & \mathcal{A}_{4,2} & 0 & 0 \end{pmatrix},$$

$$\begin{cases} \mathcal{A}_{1,3} = \dfrac{12}{4(Fr - Fr_{01})^2 + 3(Fr - Fr_{02})^2 H\rho}, \\ \mathcal{A}_{1,4} = -\dfrac{18H\rho}{4(Fr - Fr_{01})^2 + 3(Fr - Fr_{02})^2 H\rho}, \\ \mathcal{A}_{2,3} = -\dfrac{18}{H\left[4(Fr - Fr_{01})^2 + 3(Fr - Fr_{02})^2 H\rho\right]}, \\ \mathcal{A}_{2,4} = \dfrac{12\left[(Fr - Fr_{01})^2 + 3(Fr - Fr_{02})^2 H\rho\right]}{(Fr - Fr_{02})^2 H\left[4(Fr - Fr_{01})^2 + 3(Fr - Fr_{02})^2 H\rho\right]}, \\ \mathcal{A}_{3,1} = (Fr - Fr_{01})^2 - 1, \\ \mathcal{A}_{3,2} = -H\rho, \\ \mathcal{A}_{4,1} = -1/H, \\ \mathcal{A}_{4,2} = \dfrac{(Fr - Fr_{02})^2 - H}{H}. \end{cases}$$

DATA AVAILABILITY

The data that support the findings of this study are available within the article.

REFERENCES

[1]C. Jackson, "Internal wave detection using the moderate resolution imaging spectroradiometer (MODIS)," J. Geophys. Res.: Oceans **112**, C11012, https://doi.org/10.1029/2007JC004220 (2007).
[2]G. la Forgia, C. Adduce, and F. Falcini, "Laboratory investigation on internal solitary waves interacting with a uniform slope," Adv. Water Resour. **120**, 4–18 (2018).
[3]T. Maxworthy, "A note on the internal solitary waves produced by tidal flow over a three-dimensional ridge," J. Geophys. Res.: Oceans **84**, 338–346, https://doi.org/10.1029/JC084iC01p00338 (1979).
[4]A. New and R. Pingree, "Local generation of internal soliton packets in the Central Bay of Biscay," Deep Sea Res. Part A **39**, 1521–1534 (1992).
[5]D. Bogucki, T. Dickey, and L. Redekopp, "Sediment resuspension and mixing by resonantly generated internal solitary waves," J. Phys. Oceanogr. **27**, 1181–1196 (1997).
[6]J. Nash and J. Moum, "River plumes as a source of large-amplitude internal waves in the coastal ocean," Nature **437**, 400 (2005).
[7]Y. Dossmann, F. Auclair, and A. Paci, "Topographically induced internal solitary waves in a pycnocline: Secondary generation and selection criteria," Phys. Fluids **25**, 086603 (2013).
[8]G. La Forgia, C. Adduce, F. Falcini, and C. Paola, "Migrating bedforms generated by solitary waves," Geophys. Res. Lett. **46**, 4738–4746, https://doi.org/10.1029/2019GL082511 (2019).
[9]G. la Forgia, L. Ottolenghi, C. Adduce, and F. Falcini, "Intrusions and solitons: Propagation and collision dynamics," Phys. Fluids **32**, 076605 (2020).
[10]L. Ottolenghi, C. Adduce, F. Roman, and G. la Forgia, "Large eddy simulations of solitons colliding with intrusions," Phys. Fluids **32**, 096606 (2020).
[11]J. Apel, J. Holbrook, A. Liu, and J. Tsai, "The Sulu Sea internal soliton experiment," J. Phys. Oceanogr. **15**, 1625–1651 (1985).
[12]S. Sarkar and A. Scotti, "From topographic internal gravity waves to turbulence," Annu. Rev. Fluid Mech. **49**, 195–220 (2017).
[13]G. Carter, M. Gregg, and R.-C. Lien, "Internal waves, solitary-like waves, and mixing on the Monterey Bay shelf," Cont. Shelf Res. **25**, 1499–1520 (2005).
[14]R. Droghei, F. Falcini, D. Casalbore, E. Martorelli, R. Mosetti, G. Sannino, R. Santoleri, and F. Chiocci, "The role of internal solitary waves on deep-water sedimentary processes: The case of up-slope migrating sediment waves off the Messina Strait," Sci. Rep. **6**, 36376 (2016).
[15]G. la Forgia, T. Tokyay, C. Adduce, and G. Constantinescu, "Bed shear stress and sediment entrainment potential for breaking of internal solitary waves," Adv. Water Resour. **135**, 103475 (2020).
[16]K. Davis and S. Monismith, "The modification of bottom boundary layer turbulence and mixing by internal waves shoaling on a barrier reef," J. Phys. Oceanogr. **41**, 2223–2241 (2011).
[17]B. Sutherland, K. Barret, and G. Ivey, "Shoaling internal solitary waves," J. Geophys. Res.: Oceans **118**, 4111–4124, https://doi.org/10.1002/jgrc.20291 (2013).
[18]G. la Forgia, T. Tokyay, C. Adduce, and G. Constantinescu, "Numerical investigation of breaking internal solitary waves," Phys. Rev. Fluids **3**, 104801 (2018).
[19]G. la Forgia, D. Cavaliere, C. Adduce, and F. Falcini, "Mixing efficiency for breaking internal solitary waves," J. Geophys. Res.: Oceans **126**, e2021JC017275, https://doi.org/10.1029/2021JC017275 (2021).
[20]W. Alpers, P. Brandt, A. Rubino, and J. Backhaus, "Recent contributions of remote sensing to the study of internal waves in the Straits of Gibraltar and Messina," Bull. Inst. Oceanogr. Monaco-Numero Spec. **17**, 21–40 (1996).
[21]P. Brandt, A. Rubino, D. Quadfasel, W. Alpers, J. Sellschopp, and H. Fiekas, "Evidence for the influence of Atlantic–Ionian stream fluctuations on the tidally induced internal dynamics in the Strait of Messina," J. Phys. Oceanogr. **29**, 1071–1080 (1999).
[22]D. Cavaliere, G. la Forgia, C. Adduce, W. Alpers, E. Martorelli, and F. Falcini, "Breaking location of internal solitary waves over a sloping seabed," J. Geophys. Res.: Oceans **126**, e2020JC016669, https://doi.org/10.1029/2020JC016669 (2021).
[23]R. Grimshaw, D. Pelinovsky, E. Pelinovsky, and A. Slunyaev, "Generation of large-amplitude solitons in the extended Korteweg–de Vries equation," Chaos **12**, 1070–1076 (2002).
[24]N. J. Zabusky and M. D. Kruskal, "Interaction of 'solitons' in a collisionless plasma and the recurrence of initial states," Phys. Rev. Lett. **15**, 240 (1965).
[25]E. Pelinovsky, O. Polukhina, A. Slunyaev, and T. Talipova, *Internal Solitary Waves*, Solitary Waves in Fluids (WIT Press Southampton, 2007), p. 25.
[26]M. Miyata, "Long internal waves of large amplitude," in *Nonlinear Water Waves* (Springer, 1988), pp. 399–406.
[27]W. Choi and R. Camassa, "Fully nonlinear internal waves in a two-fluid system," J. Fluid Mech. **396**, 1–36 (1999).
[28]T. Kao, F.-S. Pan, and D. Renouard, "Internal solitons on the pycnocline: Generation, propagation, and shoaling and breaking over a slope," J. Fluid Mech. **159**, 19–53 (1985).
[29]H. Michallet and G. Ivey, "Experiments on mixing due to internal solitary waves breaking on uniform slopes," J. Geophys. Res.: Oceans **104**, 13467–13477, https://doi.org/10.1029/1999JC900037 (1999).
[30]J. Grue, A. Jensen, P.-O. Rusås, and J. Sveen, "Properties of large-amplitude internal waves," J. Fluid Mech. **380**, 257–278 (1999).
[31]H. Du, G. Wei, S.-D. Wang, and X.-L. Wang, "Experimental study of elevation- and depression-type internal solitary waves generated by gravity collapse," Phys. Fluids **31**, 102104 (2019).
[32]T. Kodaira, T. Waseda, M. Miyata, and W. Choi, "Internal solitary waves in a two-fluid system with a free surface," J. Fluid Mech. **804**, 201–223 (2016).
[33]G. la Forgia and G. Sciortino, "The role of the free surface on interfacial solitary waves," Phys. Fluids **31**, 106601 (2019).
[34]R. Barros and S. Gavrilyuk, "Dispersive nonlinear waves in two-layer flows with free surface. II. Large amplitude solitary waves embedded into the continuous spectrum," Stud. Appl. Math. **119**, 213–251 (2007b).
[35]R. Barros, S. Gavrilyuk, and V. Teshukov, "Dispersive nonlinear waves in two-layer flows with free surface. I. Model derivation and general properties," Stud. Appl. Math. **119**, 191–211 (2007).
[36]K. G. Lamb and D. Farmer, "Instabilities in an internal solitary-like wave on the Oregon shelf," J. Phys. Oceanogr. **41**, 67–87 (2011).
[37]L. Boegman and M. Stastna, "Sediment resuspension and transport by internal solitary waves," Annu. Rev. Fluid Mech. **51**, 129–154 (2019).

[38]M. Stastna and K. G. Lamb, "Large fully nonlinear internal solitary waves: The effect of background current," Phys. Fluids **14**, 2987–2999 (2002).
[39]W. Choi, "The effect of a background shear current on large amplitude internal solitary waves," Phys. Fluids **18**, 036601 (2006).
[40]C. Xu and M. Stastna, "Internal waves in a shear background current: Transition from solitary-wave regime to dispersive-wave regime," Phys. Rev. Fluids **4**, 094801 (2019).
[41]G. la Forgia and G. Sciortino, "Interfacial solitons propagating through a background shear current," Phys. Fluids **32**, 106603 (2020).
[42]W. R., Inc., *Mathematica*, Version 11.2 (W. R., Inc., Champaign, IL, 2017).
[43]P. L. Liu and X. Wang, "A multi-layer model for nonlinear internal wave propagation in shallow water," J. Fluid Mech. **695**, 341 (2012).
[44]R. Barros, W. Choi, and P. A. Milewski, "Strongly nonlinear effects on internal solitary waves in three-layer flows," J. Fluid Mech. **883**, A16 (2020).
[45]C. Robinson, "Melnikov method for autonomous Hamiltonians," Contemp. Math. **198**, 45–54 (1996).
[46]R. Camassa, G. Kovačič, and S.-K. Tin, "A melnikov method for homoclinic orbits with many pulses," Arch. Ration. Mech. Anal. **143**, 105–193 (1998).
[47]J. Guckenheimer and P. Holmes, *Nonlinear Oscillations, Dynamical Systems, and Bifurcations of Vector Fields* (Springer Science and Business Media, 2013), Vol. 42.
[48]W. Choi and R. Camassa, "Weakly nonlinear internal waves in a two-fluid system," J. Fluid Mech. **313**, 83–103 (1996).
[49]J. Xu, Y. He, Z. Chen, H. Zhan, Y. Wu, J. Xie, X. Shang, D. Ning, W. Fang, and S. Cai, "Observations of different effects of an anti-cyclonic eddy on internal solitary waves in the South China Sea," Prog. Oceanogr. **188**, 102422 (2020).